Journal of Physics D:
Applied Physics

TOPICAL REVIEW • OPEN ACCESS

Waveguide integrated superconducting nanowire single-photon detectors for integrated photonics

To cite this article: Vidur Raj *et al* 2025 *J. Phys. D: Appl. Phys.* **58** 243001

OPEN ACCESS
IOP Publishing
Journal of Physics D: Applied Physics
J. Phys. D: Appl. Phys. **58** (2025) 243001 (34pp)
https://doi.org/10.1088/1361-6463/add946

Topical Review

Waveguide integrated superconducting nanowire single-photon detectors for integrated photonics

Vidur Raj[1,2,*], Adan Azem[3,4], Max Patterson[1], Devendra Kumar Namburi[1], Jeff F Young[4,5,*] and Robert H Hadfield[1,*]

[1] James Watt School of Engineering, University of Glasgow, Glasgow G12 8QQ, United Kingdom
[2] Quanastra Pvt. Ltd, M-60 (First Floor), Shyam Park, Nawada, Delhi 110059, India
[3] Department of Electrical and Computer Engineering, University of British Columbia, Vancouver, British Columbia V6T 1Z4, Canada
[4] Stewart Blusson Quantum Matter Institute, University of British Columbia, Vancouver, British Columbia V6T 1Z4, Canada
[5] Department of Physics and Astronomy, University of British Columbia, Vancouver, British Columbia V6T 1Z1, Canada

E-mail: vidur.raj@quanastra.com, young@phas.ubc.ca and robert.hadfield@glasgow.ac.uk

Received 14 January 2025, revised 28 April 2025
Accepted for publication 15 May 2025
Published 29 May 2025

Abstract

Integrated photonics is expected to play a key role in the scalability of quantum systems for applications such as quantum computing, quantum communications, quantum internet, and quantum metrology. One of the primary components of quantum integrated photonics is a single photon detector, which reads out the quantum information encoded in photons. Amongst available single-photon detection schemes, superconducting nanowire single photon detectors (SNSPDs) remain the most promising technology for effective on-chip coupling, because they can be seamlessly integrated with a wide range of waveguide materials and substrates and have shown unparalleled performance from visible to the mid-infrared regime. Here, we review different aspects of SNSPDs and schemes for their on-chip integration for different integrated photonics applications. Although mostly concentrated on quantum applications, we also cover some of the important wider photonics applications including imaging, AI and machine learning, and single-photon spectroscopy, and conclude the review with a future outlook discussing emerging research areas enabled by photonic integrated circuits based on SNSPDs.

Keywords: invited, waveguide, SNSPD, integrated photonics, single photon detection, topical review

* Authors to whom any correspondence should be addressed.

1. Introduction

Since first reported by Gol'tsman and co-workers in 2001 [1], superconducting nanowire single-photon detectors (SNSPDs or SSPDs) have become synonymous with state-of-the-art single photon detection [2, 3]. They have shown unparalleled performance, particularly in the infrared regime and telecom wavelengths with high quantum efficiency (QE) (>90%), few-ps timing jitter, photon number resolution, response time of the order of tens of ns, high spectral sensitivity, and dark counts below 1 Hz [2, 4]. This, in turn, has allowed a wide range of both classical and quantum applications, including ultrafast long distance quantum key distribution (QKD) [5–7], quantum computation [8, 9], boson sampling [10, 11], quantum optics [12, 13], optical time domain reflectometry [14, 15], fluorescence lifetime imaging microscopies [16–19], and neuroimaging with unparalleled resolution [16, 20].

In parallel, photonic integrated circuits (PICs) are already revolutionizing classical technologies such as light detection and ranging (LiDAR), optical biosensing, telecommunications, data centers, augmented- and virtual-reality. Photodiodes or avalanche photodiode detectors (APD) are critical components of these classical PICs. Integrated APD technology is advancing rapidly for high-sensitivity receiver applications [21, 22]. However, for most classical applications, APDs are not typically operated in single-photon counting mode. Moreover, their performance is usually constrained by gain-bandwidth limitations and significantly affected by high dark current levels.

Most of the quantum optical applications listed above requires detectors with single photon counting and/or photon number resolving capabilities. So far, these quantum systems have been developed using *stand-alone* APDs operated in the photon counting modes (SPADs), SNSPDs, or transition edge sensors (TESs). Unsurprisingly, just as was the case in classical photonic technologies, there is a trend towards integrating several of these detectors on a single chip to improve overall processing power. One major differentiating factor for superconducting detectors is that they must operate at cryogenic temperatures. This implies that either the entire photonic chip has to be operated at cryogenic temperatures, or the detectors alone are integrated on one chip operated in a cryostat, connected to the main processing chip via optical fiber(s).

SNSPDs have demonstrated exceptional performance compared to other single-photon detection technologies, such as SPADs and TESs [9]. Especially, for applications requiring only single-photon sensitivity, SNSPDs offer clear advantages over SPADs, with higher efficiency, better timing resolution, and significantly reduced dark counts. In photon-number resolving (PNR) applications, while SNSPDs have shown promise, particularly when combined in photonic circuits, it remains an open question whether they outperform TESs for high-fidelity photon counting. Nonetheless, in comparison to other superconducting detector types, SNSPDs operate at relatively elevated temperatures (2–4 K) and integrate more readily with a wide range of waveguide materials, including foundry-compatible options such as silicon, silicon nitride, tantalum pentoxide, lithium niobate, and gallium arsenide. These capabilities, combined with their scalability and versatility, establish SNSPDs as one of the primary candidates for quantum PICs applications.

Moreover, waveguide integrated SNSPDs (WSNSPDs) have other added advantages, for example, compared to stand-alone systems, WSNSPDs allow for near-perfect absorption in a relatively smaller segment of nanowire because of enhanced interaction length between the nanowire and the waveguide. This, in turn, allows for smaller dead time and few-ps timing jitter with near-unity internal detection efficiency making them invaluable for PICs. Additionally, waveguide integration allows for capabilities such as multiplexing, ultra-low noise operation, on-chip coincidence measurements, and high-resolution spectroscopy, which is otherwise very complicated or not possible for a stand-alone SNSPD system.

Hu *et al* proposed the first scheme for integrating an SNSPD with a waveguide [23]. Since then there has been significant development and an on-chip detection efficiency (OCDE) of more than 90% has been achieved with ultra-low dark count [24, 25], and GHz count rate with ∼17 ps timing jitter [26]. Most recently, using an array of WSNSPDs, Cheng *et al* demonstrated photon resolving capability for up to 100 photons, which in turn allowed them to perform on-chip measurement of the high-order correlation function for up to 15 photons, opening a new frontier in quantum photonics [27]. In another important development in the field, PsiQuantum reported the development of wafer scale fabrication of SNSPDs with thousands of SNSPDs showing above 98% on-chip efficiency [28, 29].

In this review, we summarize some of the most recent developments in the field of WSNSPDs and anticipate future developments. Figure 1 provides figurative summary of some of the aspects covered in this review. For a general review of SNSPDs, we refer readers to [2, 4, 30–37]. The present review both updates previous reviews on WSNSPDs [38–41], and complements those reviews by providing the most recent developments in the field and covers some other aspects that were not covered in those reviews. We begin by summarizing the general theoretical concepts of SNSPDs and the impact of various physical processes on key performance metrics of SNSPDs (section 2). In subsequent sections (sections 3 and 4), we discuss some of the most recent developments relevant specifically to WSNSPDs, such as waveguide fabrication technology, materials for waveguides, different schemes for on-chip fiber coupling, superconducting materials for SNSPDs, schemes for photon number resolution, and schemes for extending SNSPDs operation to the mid infrared (mid-IR) regime. In section 5, we discuss applications of WSNSPDs giving a perspective on both quantum and classical applications. Finally, before concluding the review, we include a future outlook section, discussing some of the foreseeable developments in the field of waveguide integrated photonics, and the future potential of WSNSPDs in revolutionizing different sectors of photonics technology.

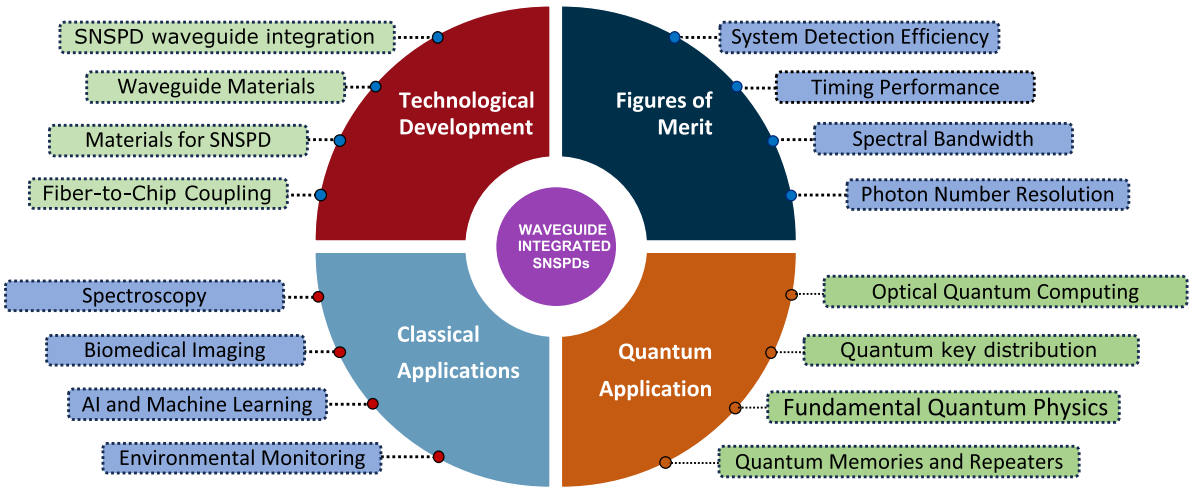

Figure 1. A figurative summary of some of the aspects covered in this review.

2. Key concepts

This section describes phenomenological model concepts that have been used to fit various SNSPD response data. These models are based on the fundamental superconducting properties of the material used to form the nanowire. It then identifies mechanisms that need to be considered when designing the layout of the nanowire and finishes with readout-circuit related considerations.

2.1. The detection mechanisms

The detection mechanism of SNSPDs can be categorized into two regimes- (a) the high-photon energy limit, where the photon energy striking the nanowire is much greater than 2Δ, and (b) the low-photon energy limit, where the photon energy is just above 2Δ. Here, 2Δ represents the superconducting gap energy.

2.1.1. The high photon energy limit. According to the Bardeen–Cooper–Schrieffer (BCS) theory, materials transitioning into superconductors at sufficiently low temperatures develop an electronic bandgap with energy on the order of a few meV. These materials typically exhibit critical temperatures (T_c) ranging from a few to tens of degrees Kelvin. The energy gap reaches its maximum value at 0 K, and as the temperature approaches T_c, the bandgap diminishes. This behavior is summarized by the following equation derived from BCS theory:

$$2\Delta\,(T = 0\ \mathrm{K}) = 3.53 k_b T_c \tag{1}$$

$$2\Delta\,(T \to T_c) \approx 3.07 k_b T_c \sqrt{1 - \frac{T}{T_c}}. \tag{2}$$

The ability of a superconducting strip to detect a single photon arises from the fact that if the energy deposited by the photon exceeds 2Δ, it results in the breaking of Cooper pairs, causing a localized suppression of superconductivity. This disruption in the superconducting state is the fundamental mechanism behind photon detection in superconducting nanowires. For example, a photon with energy 1 eV (1240 nm) should be able to break several hundred Cooper pairs, whose binding energy is on the order of a few meV.

The degree to which the superconducting state is disrupted depends on the density of broken Cooper pairs, as this determines the reduction in the local superconducting energy gap. Notably, it is the density of broken pairs, rather than their total number, that governs the response. In such scenarios, the 'hotspot' model (see figure 2(a)) offers a straightforward and effective framework for understanding the dynamics of nanowire conductivity. This model has been instrumental in explaining experimental observations.

The hotspot model presumes the energy absorbed by the electrons can establish a local quasi-thermal distribution at a temperature above ambient, within a thermalization timescale τ_{th} [42]. In this simplified model, the suppression of the superconducting state occurs within a volume determined by the ratio of the thermalization time to the thermal diffusion time. The latter, denoted as $\tau_{D,w} \cong {w^2}/{4D}$ [43], where w represents the width of the nanowire and D is the diffusion coefficient. This parameter characterizes the rate at which heat dissipates within the electron system from the absorption site. A small diffusion coefficient (i.e. longer thermal diffusion time) ensures fast thermalization by confining the energy of an absorbed photon to a relatively small volume during the initial stages of hot-spot formation, improving sensitivity of SNSPDs. A small diffusion coefficient also ensures shorter electron–electron inelastic relaxation time, which further reduces the thermalization time, and improves

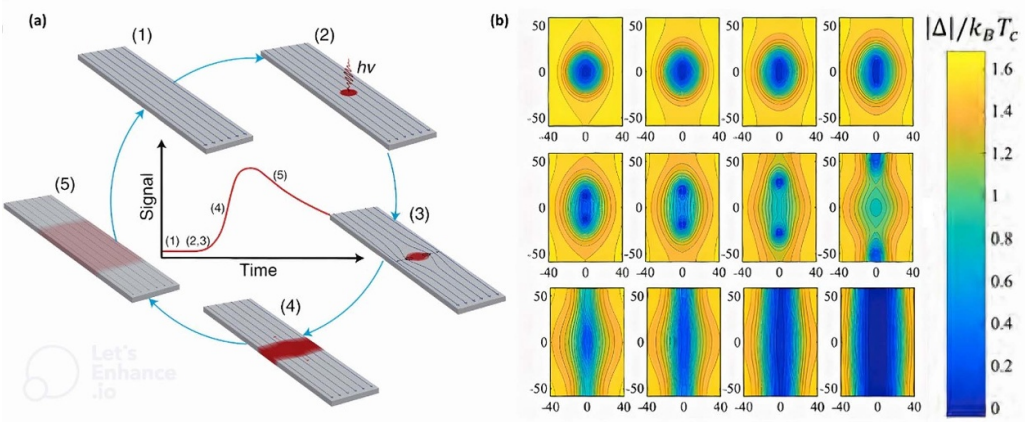

Figure 2. (a) A simplified schematic of hotspot detection mechanism for SNSPDs. Reproduced with permission from [3]. Copyright © 2020, Springer Nature Limited CC BY-NC 4.0. (b) The evolution of the order parameter of a superconducting strip of width of 120 nm followed by the formation of a vortex-antivortex pair, and their motion afterwards to the edges, suppressing the superconductivity. This suppression of superconductivity leads to the formation of a normal domain in the strip. The current flow is from left to right. Reprinted figure with permission from [44], Copyright (2019) by the American Physical Society.

SNSPDs ability to detect single photon. Similarly, the nanowire width is kept small to ensure remains larger than the τ_{th} [43].

If the thermalization time is shorter than the diffusion time, the superconductivity could be initially suppressed over an area of diameter less than the nanowire width [43]. This scenario is depicted in figure 2(a), wherein the superconducting state is initially suppressed only over a fraction of the wire width, which results in the current density passing around the hotspot to increase. Since the biasing current is usually more than 80% of the critical current, it accelerates the loss of superconductivity in nearby areas, causing the quenching to happen faster than it would if limited solely by thermal diffusion.

2.1.2. Low photon energy limit. For longer wavelength photons that might only be capable of breaking a few Cooper pairs, a more sophisticated model is required. When the absorbed photon energy is only slightly above 2Δ, the model has to be augmented to include non-dissipative suppression of superconductivity through mechanisms such as vortex-antivortex pair (VAP) unbinding, vortex entry, vortex nucleation, or phase slip (see figure 3(a)) [36, 45]. These vortex dynamics do not play a large role at higher photon energies because they are destroyed in the cascaded Cooper pair breaking process [46]. With reference to figure 2(b) [47], Allmaras showed through detailed simulation that if the absorption is at the center of the nanowire, the VAP unbinds toward the edges of the strip, whereas, in cases where photon absorption occurs near the edges of the nanowire, the vortex enters from the edges traversing through the nanowire strip [47]. In either case, the superconductivity is suppressed due to energy dissipated in the movement of vortices. Using a probabilistic vortex crossing and nucleation model, Jahani *et al* was able to show saturating QE at lower energies with exponentially decreasing QE beyond cutoff wavelengths, which the hotspot model failed to explain (see figures 3(c) and (d)) [48]. Table 1 provides a summary of the various theoretical models developed to describe the behavior of SNSPDs across different operational regimes.

2.1.3. Vortex dynamic and dark counts. Vortex dynamics also play a role in the detector's dark count rate. As per the Berezinskii–Kosterlitz–Thouless superconducting transition model, below $T_{c,}$ vortices transition into VAPs of different sizes [49, 50]. As shown in figure 3(b), when a current flows through the superconductor, no net Lorentz force is applied to the VAPs, as the applied forces are opposite in direction for the two components of the VAP [51]. However, the bias tends to align the pairs orthogonal to the applied current to attain a minimum energy (U_{min}) given by [46]:

$$U_{\text{min}} = \frac{\pi^2 \hbar \Delta}{2e^2 R_s}\left(\beta + \frac{I_{\text{bias}}}{2.6\varepsilon I_c} + \frac{1}{\varepsilon}\cdot \ln\left(\frac{2.6 I_c}{I_{\text{bias}}}\right)\right)\tanh\left(\frac{\Delta}{2k_b T}\right). \tag{3}$$

Here, β and ε are model parameters, and R_s is the normal sheet resistance of the film. The dark count rate (DCR) is proportional to the probability of VAP unbinding, which scales with $\exp\left(-U_{\text{min}}/k_b T\right)$. As shown in the above equation, the U_{min} depends on Δ, and absorption of photons reduces Δ to temporarily increase the probability of VAP unbinding, leading to an increased DCR in the presence of photons.

For a more thorough treatment of the impact of vortices on SNSPD performance, the interested reader is referred to [43, 47, 49, 50].

Finally, in the limiting case of ultrathin nanowires, where vortices are not supported, suppression of superconductivity happens through 1D phase slip [47].

In addition to theoretical consideration mentioned above, design of WSNPD must also account for nanowire kinetic inductance [52–54], and current crowding effects [55, 56], both of which play a crucial role in performance optimization.

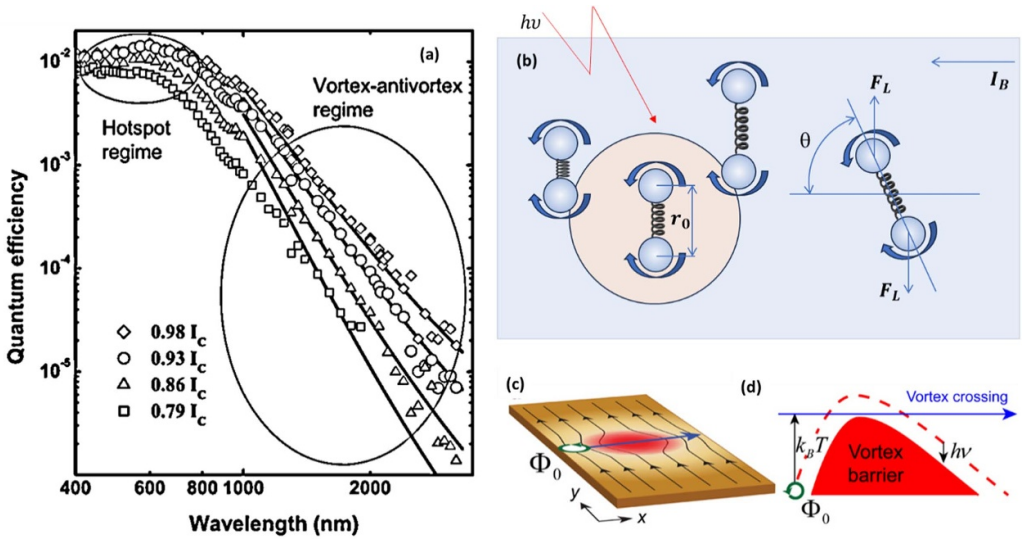

Figure 3. (a) Quantum efficiency as a function of wavelength at different bias currents. For high energy photons, SNSPD behavior follows the hotspot model, whereas for low energy photons, SNSPD behavior follows the vortex-antivortex model. (b) The role of bias current in aligning the vortex-antivortex pairs (VAPs) at right angle to the direction of current flow. The VAP binding energy is a function of θ and reaches its minimum when the VAP aligns with the current axis at 90°. The circle with radius r_0, depicts the non-equilibrium region created during the photon absorption by the detector. (a), (b) Reprinted from [46], Copyright (2008), with permission from Elsevier. (c) In reference 18, Jahani *et al* propose movement of vortices across the nanowire due to the forces exerted by applied bias current. However, the movement of these vortices is probabilistic, and the probability of a vortex crossing enhances after photon absorption due to reduced vortex potential barrier, which in turn depends on quasi-particles multiplication and the bias current. (d) Illustrates that prior to photon absorption, the vortex potential barrier effectively restricts the movement of vortices. However, after photon absorption, this barrier weakens, increasing the likelihood of thermally excited vortices overcoming the barrier and crossing the width of the nanowire. (c), (d) Reprinted from [48], with the permission of AIP Publishing.

Table 1. Different theoretical models and their mechanism summary.

Model name	Mechanism summary (Applicability)
Hotspot model	Photon absorption creates a localized resistive hotspot, disrupting Cooper pairs and leading to superconductivity suppression across the nanowire width. Applicable to high-energy photons. **(Applicable when Photon Energy $\gg 2\Delta$)**
Vortex-antivortex model	Photon absorption induces vortex entry or vortex-antivortex pair (VAP) formation. Vortices move across the nanowire, dissipating energy and impacting superconductivity. Effective for low-energy photons where vortex dynamics are prominent. **(Applicable when Photon Energy $> 2\Delta$)**
Phase slip model	Photon absorption in ultra-thin nanowires where vortex dynamics are absent. Superconductivity is suppressed by phase slips in the nanowire, resulting in local resistance increases. **(Applicable for ultrathin nanowire when Photon Energy $> 2\Delta$)**
Probabilistic vortex model	Photon absorption increases the probability of vortex crossing, influencing superconductivity through probabilistic vortex movement across the nanowire. **(Yet to be experimentally verified)**

3. SNSPD performance parameters

In the previous section, we explored key considerations and models essential for designing an SNSPD. In the following section, we will briefly examine critical performance parameters, including QE, dark count rate, dead time, timing jitter, spectral bandwidth, and photon number resolution.

3.1. System detection efficiency (SDE)

Before defining SDE, it is essential to discuss the various efficiency metrics commonly reported in SNSPD literature. These include:

- QE: the probability that an incident photon is absorbed by the superconducting nanowire and generates a detectable response. This efficiency is primarily dictated by the optical absorption properties of the nanowire material and its geometry.
- Intrinsic detection efficiency (IDE): the probability that an absorbed photon successfully triggers a detection event, given that absorption has already occurred. IDE depends on factors such as bias current, operating temperature, and photon energy.
- SDE: the overall probability that an incident photon leads to a recorded detection event. SDE incorporates all losses in the system, including optical coupling inefficiencies, reflection

losses at interfaces, propagation losses in optical fibers or waveguides, as well as the combined effects of QE and IDE.

SDE, which quantifies the likelihood that photons emitted from a source are detected by the system, is one of the most critical performance metrics for any detection setup. It is typically expressed as the product of coupling efficiency, absorption efficiency, internal QE, and counting electronics efficiency, and is given as:

$$\mathrm{SDE} = \eta_{\mathrm{coupling}} \cdot \eta_{\mathrm{absorb}} \cdot \eta_{\mathrm{internal}} \cdot \eta_{\mathrm{trigger}} \,. \tag{4}$$

To limit the scope of this review we refer the readers to [57] for more details on the above-mentioned individual efficiencies.

For waveguide-coupled single-photon detectors, the OCDE is more commonly reported than the SDE because, in a waveguide-integrated SNSPD, the coupling efficiency can be tuned separately, and does not directly affect the performance of the SNSPD.

3.2. Dark count rate and noise equivalent power (NEP)

DCR refers to detection pulses that do not originate from the absorption of single photons intentionally sent to the SNSPD. The origin of dark count can be extrinsic (counts due to leaked light, thermal radiation of the fiber, or blackbody radiation from the ambient environment) or intrinsic (a property of narrow superconducting wires) in nature. For SNSPDs, very low dark counts (i.e. of the order of less than one count per second) are typically reported. For stand-alone systems, using cold optical filters, the dark counts can be significantly reduced to less than 0.1 counts per second, making them very useful for quantum communication applications [58].

Waveguide-integrated SNSPDs are naturally less prone to extrinsic dark counts because the waveguide does not allow efficient coupling of stray light into the SNSPD, and the input port of light is relatively farther apart from the SNSPD coupling region. However, in practical applications, where pump lasers are used, more careful engineering may be required to prevent stray light leaking into the SNSPD waveguide. Waveguide-integrated SNSPDs can be more prone to intrinsic dark counts because of sharp bends and relatively complex fabrication steps. Nonetheless, DCR as low as 10^{-3} counts per second has been achieved for waveguide-integrated SNSPDs, without significantly compromising the efficiency [24].

An important figure of merit for single-photon detectors is the NEP, which is the direct measure of signal-to-noise ratio (SNR) of a single-photon detector, and is correlated to both SDE and DCR, as follows:

$$\mathrm{NEP} = h\upsilon * \frac{\sqrt{2 * \mathrm{DCR}}}{\mathrm{SDE}} \,. \tag{5}$$

3.3. Timing jitter

Timing jitter is another important parameter of consideration for single-photon detectors, especially for applications based on time-correlated single-photon counting such as LiDAR, fiber temperature sensing, QKD or space optical communications. In high clock rate QKD, timing jitter can also contribute to the quantum bit error rate (QBER) [59–61]. SNSPD has emerged as the only detector that can achieve near 100% QE in the single-photon regime, while maintaining the timing jitter in the range of tens of ps.

The measured system timing jitter, J_{system} for an SNSPD includes contributions from the nanowire itself, J_{SNSPD}, the laser source, J_{laser}, the synchronization signal, J_{SYNC}, and the single photon counting electronics, J_{SPC}, and can be written as follows [62]:

$$J_{\mathrm{system}} = \sqrt{J_{\mathrm{SNSPD}}^2 + J_{\mathrm{laser}}^2 + J_{\mathrm{SYNC}}^2 + J_{\mathrm{SPC}}^2}. \tag{6}$$

The J_{SNSPD} is largely influenced by the hotspot dynamics, that in turn relates to rates of electron–electron inelastic scattering, electron–phonon scattering, electron diffusion and phonon escape, and geometric jitter (timing variation due to photon absorption position). Geometric jitter can often be small in waveguide-integrated detectors with short nanowires, due to their small length and area. In the case of waveguide coupled SNSPDs most of the intrinsic timing jitter is due to geometric non-uniformities (for example during growth), Fano fluctuations, and fabrication imperfections. A more recent analysis of the origin of SNSPD timing jitter can be found in [44].

The overall system jitter, J_{system} is therefore often dominated by the extrinsic sources. Given its importance in the context of SNSPDs, there has been extensive research in understanding the origin of timing jitter in SNSPDs, putting a lower limit on intrinsic SNSPD timing jitter, more details can be found in [62–67]. Bandwidth and noise figures of the readout amplifiers can have significant impact on the overall timing jitter. In this regard, cryogenic amplifier has been used to achieve low timing jitter [68].

3.4. Dead time

Dead time is the period after the detection of a photon within which the SNSPD cannot detect another photon. Several different parameters influence dead time, including material properties such as kinetic inductance and superconducting energy gap, substrate, nanowire geometry, and readout circuitry. In general, higher kinetic inductance leads to longer dead times, but smaller kinetic inductance can lead to latching, therefore, the kinetic inductance of SNSPDs should be optimum for maximum performance.

3.5. Spectral bandwidth

The hotspot and thermalization process influences the SNSPD's cut-off wavelength and internal detection efficiency at any given wavelength. The internal detection efficiency of SNSPDs depends on nanowire cross-section, bias current, and quantum yield. Quantum Yield in this case describes how efficiently the absorbed photon energy leads to the creation of a

resistive 'hotspot' that can disrupt the superconducting state to produce a measurable electrical pulse. As per Engel and Schilling the criteria to achieve unity internal detection efficiency at a given wavelength is met when the normal hotspot diameter satisfies the following conditions [69]:

$$2R_{\mathrm{hs}} \geqslant w\left(1 - {I_{\mathrm{bias}}}/{I_{\mathrm{c,dep}}}\right) \tag{7}$$

where R_{hs} is the maximum diameter of the hotspot, w is the nanowire width and ${I_{\mathrm{bias}}}/{I_{\mathrm{c,dep}}}$ is the bias current normalized to the depairing critical current. Although the equation predicts that below a certain R_{hs} the internal detection efficiency should reduce sharply to zero, the transition is not sharp but rather vanishes gradually, as already discussed in detail in section 2 and depicted in figure 3(a). This behavior has been explained in terms of the superconducting state fluctuations, due to the probabilistic nature of VAP unbinding, vortex nucleation, vortex entry, or phase slip, which determines the expansion of the hotspot [48, 51, 70].

Nonetheless, estimating R_{hs} can help design SNSPDs. In another paper, Semenov *et al* provided an equation to numerically calculate the hotspot diameter in an infinitely large superconducting strip, written as follows [71]:

$$R_{\mathrm{hs}} = \sqrt{\zeta \frac{h\nu}{\Delta} \frac{1}{2D\tau_{\mathrm{th}} d N_0 \Delta}} \left(\frac{1}{\pi^4 N_0 \Delta}\right)^{\frac{1}{3}} \times \ln\left(1 + \pi^2 \zeta \frac{h\nu}{\Delta} \frac{1}{D\tau_{\mathrm{th}} d N_0 \Delta}\right) \tag{8}$$

here ζ is a material dependent experimental parameter (efficiency of the quasi-particle multiplication) accounting for losses during hotspot formation and quasiparticle multiplication, Δ is the temperature-dependent superconducting bandgap, D is electron diffusivity, τ_{th} is the electron thermalization time, N_0 is the density of states for electrons near Fermi energy, and d is the thickness of the superconducting strip.

3.6. Photon number resolution

Photon number resolving detectors are critical for quantum information processing, optical quantum computing, boson sampling, and metrology applications. However, SNSPDs in its most simple form is known as click, or bucket detectors, meaning they can distinguish between zero and non-zero photons regardless of the photon number. They also lack photon energy resolving capabilities. However, the limited energy resolution and absence of photon number resolution in conventional SNSPDs can be addressed through high-impedance readouts [72], by proper impedance-matching between the nanowire and the coaxial transmission line [73], and innovative multiplexing techniques such as parallel nanowire detectors [74], series nanowire detectors [75, 76], time-bin multiplexing [77], and delay-line multiplexers [12]. In addition, advanced characterization techniques can be used to readout information embedded in the rising edge of the detection pulses instead of their amplitude. Many of these methods have been extensively discussed by Mattioli *et al*, [32] and we direct readers to their review for further details, given the limited scope of this discussion. Several of these methods have already been covered in detail by Mattioli *et al* [32], and we refer readers to the review for further information given limited scope of the review.

4. Technological development

In this section, we summarize recent advancements in waveguide-integrated SNSPD technologies. Starting with integration schemes, we review developments in materials for both waveguides and SNSPDs. The discussion extends to circuit-level innovations and packaging strategies, which are increasingly critical as the field advances. These developments address the growing complexity of applications (as reviewed in section 5) and the need for scalable, reliable solutions to meet practical requirements in quantum and classical photonics.

4.1. Schemes for SNSPDs integration on waveguide

Figure 4 shows some of the different ways in which an SNSPD can be integrated with a waveguide. In case of WSNSPDs, the light propagating along the waveguide is coupled to the superconducting nanowire through the evanescent component of the guided waveguide mode. The absorbed fraction of the incident guided light in the nanowire is typically estimated using finite time domain 3D numerical solvers of the Maxwell equations. In the case of relatively long U-shaped nanowire geometries (travelling wave detection), the rate of absorption is characterized by the incremental contribution of the nanowire to the imaginary part of the guided mode's propagation constant in the otherwise near lossless waveguide. The incremental contribution of the nanowire to the real part of the mode's propagation constant is typically negligible, so reflections at the interface between the bare and coated waveguides can typically be ignored for thin nanowires [25].

Pernice *et al* showed that in the traveling wave geometry, NbN nanowire lengths of the order of tens of microns atop a silicon-on-insulator (SOI) waveguide is required to achieve near unity absorption, with the absorption increasing approximately 1 dB per micron (see figure 4(a)) [25]. This is already a significant improvement over fiber-coupled SNSPDs, which require long nanowires (several hundred micrometers in length) to match the fiber's beam diameter and rely on an optical cavity for enhanced light absorption. In contrast, waveguide-integrated SNSPDs achieve efficient absorption through evanescent coupling, enabling shorter nanowires, reduced dead time, and improved timing jitter without the need for complex cavity structures. This makes them more scalable and better suited for integrated photonic circuits. This length can further be reduced by using a ring resonator or a photonic crystal resonator. For example, Akhlaghi *et al* patterned holes in a silicon nanobeam (SOI substrate, 190 nm thick and 500 nm wide waveguide) to create a 2D asymmetric optical microcavity around the nanowire and near-perfect

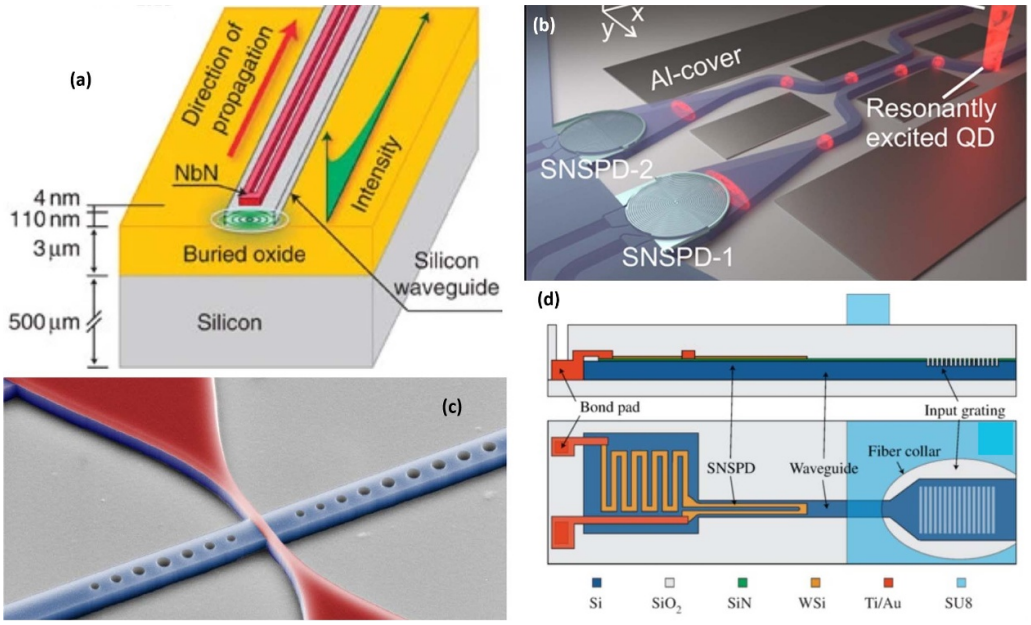

Figure 4. Different schemes for waveguide coupling with SNSPDs. (a) A NbN SNSPD positioned on a SOI ridge waveguide, illustrating that the light absorption occurs along the direction of light propagation, with a significant portion of the light being absorbed within a few tens of microns. Reproduced with permission from [25]. Copyright © 2012, The Author(s) CC BY-NC-ND 3.0 (b) A large area spiral SNSPD coupled to an inverse tapered waveguide. Reprinted with permission from [83]. Copyright (2018) American Chemical Society. (c) An SNSPD atop a 1D photonic crystal cavity enhanced absorption in less than a micron length. Reprinted with permission from [79]. Copyright (2016) American Chemical Society. (d) A U-shaped waveguide integrated SNSPD integrated with an on-chip inductor to prevent latching. Reprinted figure with permission from [87], Copyright (2020) by the American Physical Society.

absorption of light was achieved in a very short section of nanowire [78]. However, they reported a recovery time of ∼7 ns, and a timing jitter of ∼55 ps, which is still relatively high for such a short section of the nanowire, most probably because of the low SNR due to the small length and very narrow width of the nanowire. Another aspect of such a design is the very narrow spectral bandwidth operation, which can be both good or bad depending on the application. Using a similar concept, Vetter *et al* reported an SNSPD on an SOI platform with a recovery time of ∼510 ps and a low timing jitter of ∼32 ps, thus showing potential for GHz count rates [79]. They further improved this design using a 2D photonic crystal to realize a recovery time of 480 ps, with very low dark count rates, and on-chip detection efficiencies of almost 70% at telecom wavelengths [80]. Other works that use 2D photonic crystal for light trapping in SNSPDs can be found in [81, 82]. However, there can also be cases where one may require a large area SNSPD integrated atop the waveguide. Schwartz *et al* reported a tapered waveguide structure to couple the single photon from a quantum dot to a spiral-shaped SNSPD (see figure 4(c)) [83]. In this scheme, the width of the waveguide broadens from a few hundred nanometers to about 10 micrometers, as it extends to the region containing a spiral SNSPD. Moreover, waveguide coupled SNSPD also provides the opportunity for direct integration for a quantum dot based single photon source with an SNSPD [83].

Another way in which the trade-off between recovery time and absorption efficiency can be dealt with is by laying an SNSPD atop or inside of a resonant ring cavity (see figure 4(c)). Similar to photonic crystal cavities, they are also limited in terms of bandwidth but can achieve GHz rate detection rates with very low dark count owing to the cavity structure [84]. In this case, at a resonance condition, the light from a bus waveguide can be coupled to a travelling wave, ring-like resonator wherein it can circulate and interact with the nanowire many times before being fully absorbed by a small section of the SNSPD. Rhazi *et al* showed that to achieve high performance, the length of the SNSPD needs to be optimized very carefully [85]. They showed that if the length is too small, the light needs to take several round trips across the racetrack before being absorbed, degrading the temporal performance of the SNSPD. For example, they theoretically showed that a jitter as low as 0.2 ps is predicted for a nanowire of 10 μm, but the jitter degrades to 10 ps for a nanowire of 1 μm inside an SOI waveguide racetrack resonator cavity [84, 85]. Here, we would like to clarify that the 0.2 ps jitter value refers exclusively to the calculated contribution from the optical cavity, and does not represent the total device jitter, which includes additional contributions such as hotspot dynamics and readout noise. Most recently, Sánchez–Postigo *et al* proposed the subwavelength grating metamaterials for improved performance of on-chip SNSPD [86].

Waveguide integration of SNSPDs also allows new on-chip features. For example, Buckley *et al* used a branching tree structure to uniformly illuminate several SNSPDs

at the same time for application in neuromorphic computing. They were able to couple up to 15 detectors to a single integrated photonic circuit with almost all of them having a detection plateau showing 100% internal detection efficiency [87]. Additionally, similar to meander SNSPDs, waveguide-integrated SNSPDs are also polarization sensitive, and they generally show higher absorption for the either fundamental TE or TM mode [88]. To overcome this limitation, Sahin *et al* integrated an SNSPD atop a wider GaAs ridge waveguide capable of supporting both TE and TM modes [89]. The polarization independent efficiency between nanowires allowed them to place the two nanowires side-by-side to achieve similar performance from both in an on-chip second-order intensity ($g^{(2)}(\tau)$) auto-correlation experiment [89]. In another scheme, Li *et al* proposed a polarization rotator to convert incident TE_0 mode light into TM_0 mode, which allowed them to achieve near 100% absorption in about 5 μm long SNSPD [90]. Similar geometries are relevant in cases where polarization filtering is required before sending the light to the SNSPD. Another report on waveguide integration of SNSPD for polarization independent performance can be found in [91].

4.2. Waveguide materials

When designing integrated photonic systems, the choice of materials for both waveguides and superconducting nanowires plays a critical role. While the subsequent section focuses on superconducting materials, this section explores the materials suitable for waveguide fabrication. The selection criteria for waveguide materials include factors such as modulation speed and efficiency, compatibility with on-chip light sources and detectors, optical non-linearity, refractive index contrast, fabrication complexity, intrinsic losses, transparency window, and minimal background fluorescence.

Commonly used waveguide platforms for integration with SNSPDs include silicon, SOI, silicon nitride, lithium niobate (both bulk and on insulator), indium phosphide, and GaAs on AlGaAs. Additionally, materials such as diamond, aluminum nitride, silicon nitride, and tantalum pentoxide are gaining interest due to their wide bandgap, which reduces parasitic absorption and enhances transparency across broad spectral ranges. A comparative summary of the advantages and limitations some of these materials is provided in table 2. A more detailed discussion on waveguide materials is beyond the scope of this review and can be found in referenced works [111–117]. We also refer readers to [41], for a discussion on waveguide material platforms in the context of SNSPDs.

4.3. Superconducting materials and nanowire geometries

In terms of materials development for SNSPDs, the majority of the research work carried out so far has focused on NbN and NbTiN due to the robust superconducting thin film properties and ability to sustain a hotspot on photon absorption (unlike common elemental superconductors used in quantum devices such as Nb and Al). Moreover, NbN and NbTiN offer relatively high superconducting critical temperatures, which allows for their direct integration with commercially available cryocoolers operating between 2–4 K [52]. Their IDE can be relatively easily saturated at wavelengths within and below those prevalent in silicon-based integrated circuits, using nanowire widths $\sim$50 nm, that are relatively robust to fabrication variations. There are several dedicated research articles and reviews discussing their properties and deposition on different substrates relevant to waveguides [98, 118].

Both NbN and NbTiN are mainly deposited by sputtering, and it remains the preferred thin film deposition technology. One of the prime benefits of sputtering is that allows for wide range of control in stoichiometry, optical properties, and crystallinity of deposited thin film, which in turn affects the working of SNSPD [119]. Given its importance, the deposition of NbN using sputtering has been widely covered in a journal articles, and given the limited scope of the review, we refer readers to [119–122] for more details.

In recent years, atomic layer deposition (ALD) has been gaining a lot of traction because using ALD very precise thickness and stoichiometry control can be achieved across large area (see figure 5). Most recently, we reported highly uniform NbN deposited using ALD at 250 °C across 8 inch silicon wafer [123]. In another report, authors reported on-chip SOI integrated NbN SNSPD using ALD with more than 99% yield [28, 29].

In recent years, there has been a strong push to extend the spectral sensitivity of SNSPDs into the mid-IR wavelength range from $\sim$2 μm to 20 μm, motivated by applications in astronomy [124], dark matter searches [125], LiDAR and remote sensing, [2] quantum computing [126], and molecular dynamics and chemistry research [127]. Since several gas molecules exhibit sharp vibrational and rotational transitions in the mid-IR spectrum (see figure 6), mid-IR SNSPDs hold promise for applications in environmental monitoring, process control, and medical diagnostics. Several reviews have covered various aspects of mid-IR SNSPDs in specific application areas [17, 124, 127, 128].

As the wavelength of the incident photon increases, the IDE of the SNSPD decreases. This is reflected in the shrinkage or disappearance of the saturation region in the photon count rate curve. To address this, significant efforts are being made to enhance single photon sensitivity while maintaining saturated behavior. According to equation (8), several approaches can be employed to increase the hotspot radius, which is equivalent to lowering the cut-off energy of an SNSPD: (1) decreasing the nanowire's cross-sectional area, (2) increasing the critical current, (3) reducing the superconducting gap energy, (4) decreasing the density of states at the Fermi level, (5) reducing normal state diffusivity, or (6) reducing electron thermalization time. Roles of these individual parameters along with different ways to control them are summarized

Table 2. Comparison of waveguide materials for SNSPD integration: spectral ranges, advantages, and limitations.

Waveguide material (spectral range)	Advantages	Disadvantages	Use in waveguide integrated SNSPD
Silica on silicon waveguide (0.2 μm–3.5 μm)	• Low cost • Extremely low loss	• No active functionality	[92]
Silicon on insulator (1.2 μm—3.7 μm)	• Well established manufacturing process • Most mature platform • Ease of optical/electronic integration • Small size (high refractive index contrast) • Compatible with foundry fabrications	• Difficult to get light in or out at short (visible or near-infrared) wavelengths	[25, 93]
Lithium niobate (0.35 μm—5 μm)	• Excellent modulation function • Non-linear operation	• Low damage threshold	[26, 65, 94–97]
Silicon nitride (0.4 μm–7.0 μm)	• Low loss • Optical transparency from UV to mid-IR • Compatible with foundry fabrications.	• Material properties are highly process dependent	[24, 98–104]
Tantalum pentaoxide (0.25 μm–8.5 μm)	• Wide bandgap • Low self-fluorescence • Easy fabrications	• Not enough data—still an emerging material	[105]
GaAs (0.9 μm–17 μm)	• Easy light source integration • Single- and entangled-photon generation by radiative recombination. • High refractive index contrast	• High cost at the manufacturing level • Process steps may be foundry incompatible	[83, 106–108]
InP (0.95 μm–9 μm)	• Easy light source integration • High refractive index contrast	• High cost at the manufacturing level • Processes can be foundry incompatible	[108]
Diamond (UV to RF, except dips at 2.6 μm and 6.2 μm)	• Large transparency window and wide tunability of single photon source • Exceptional thermal, optical, and mechanical properties	• Fabrication and integration complexity	[103, 109]
AlGaAs on insulator (Tuneable based on Aluminum concentration)	• Ultrabright single photon source • Both linear and non-linear optical functionalities • Possibility of high thermos-optic and electro-optic modulation	• Instability of aluminum in AlGaAs can hamper long term stability	[110]

in table 3. We first discuss progress based on modifying the nanowire geometry (1), and then cover alternate superconducting materials that address one or more of the fundamental properties, (2)–(6).

(1) A reduced cross-sectional area would increase the probability of generating a hotspot for a given absorbed photon energy, as the energy per unit area is higher. Additionally, the thermal conductivity along the length of the nanowire is smaller, resulting in more localized energy deposition within the nanowire. However, this approach poses challenges because reducing the nanowire dimensions limits the switching current and consequently limits the operating bias current. As the SNSPD signal is proportional to the bias current, a reduced bias current results in a poorer SNR, imposing more stringent requirements on the readout circuit. Cryogenic amplifiers offer one means of mitigating this penalty. Moreover, reduction of the nanowire cross-section imposes stricter requirements on nanofabrication tolerances as a narrower nanowire is highly likely to suffer from constrictions and become very sensitive to edge roughness. This sensitivity significantly limits the switching current [124], and might prevent achieving a unity internal detection efficiency, potentially affecting the yield and

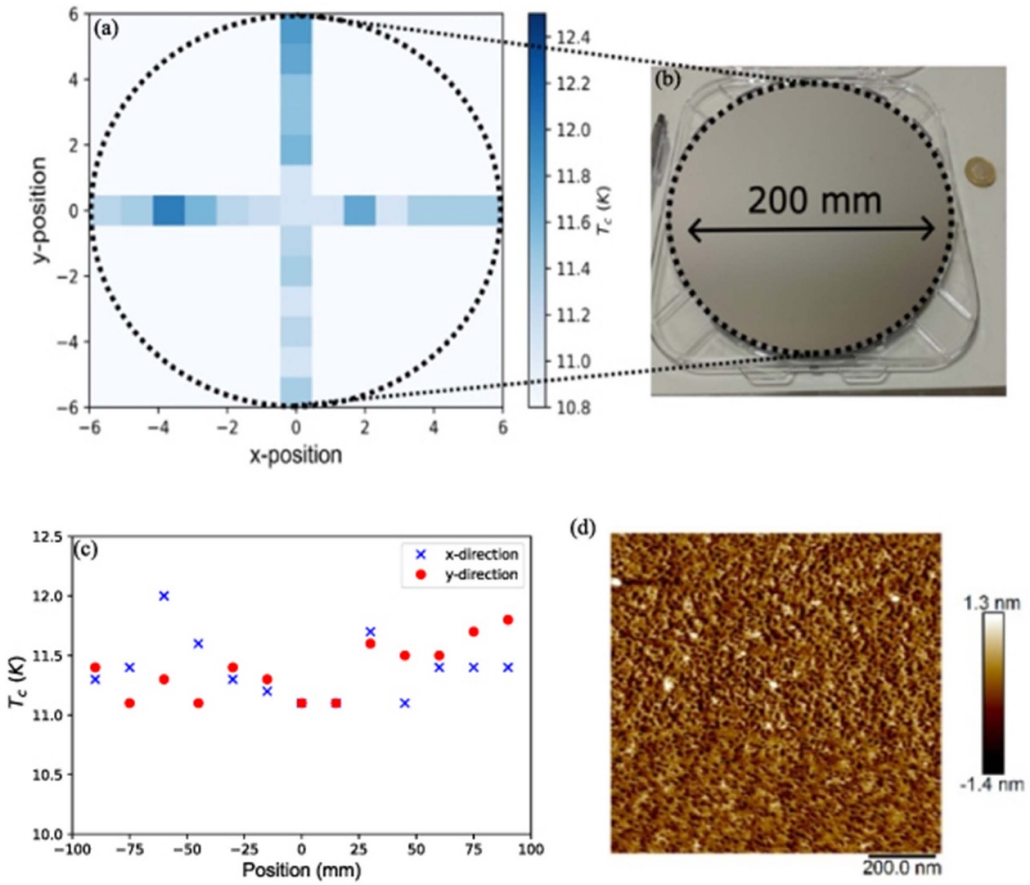

Figure 5. Highly uniform deposition of ALD superconducting NbN thin-film. (a) Shows the variation in the transition temperature across length and breadth of NbN thin-film deposited on a 200 mm wafer shown in (b). (c) The critical temperature is almost constant along the length of the wafer. (d) RMS surface roughness of a thin film measured by atomic force microscope. Reproduced from [123]. CC BY 4.0.

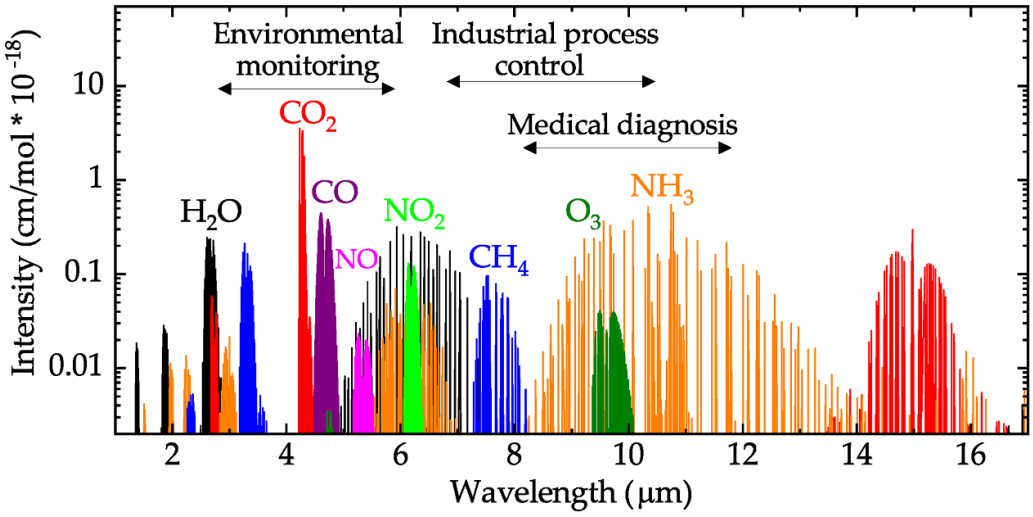

Figure 6. Mid-IR spectrum has signature absorption peaks for several gases, and measurement of these can enable a range of applications ranging from environmental monitoring to industrial process control to medical diagnostics. Reproduced with permission from [129]. Copyright © 2017, The Author(s) CC BY-NC-ND 4.0.

quality of fabricated SNSPDs. Therefore, designs should be balanced between the detector's spectral sensitivity and fabrication capabilities.

Early studies focusing on narrow nanowires compared NbN-based SNSPD composed of 70 parallel 54 nm-wide nanowires with a conventional meander-shaped SNSPD of

Table 3. Different parameter considerations for Mid-IR single photon detection.

Parameter	Description	Optimization recommendations for mid-IR
Hotspot diameter (R_{hs})	Influences cut-off wavelength and intrinsic detection efficiency (IDE). Depends on material and nanowire geometry.	Use smaller bandgap materials to increase R_{hs} for longer wavelengths. Tune material properties to enhance quasi-particle multiplication efficiency.
Nanowire width (w)	Influences detection efficiency, and dark count.	Optimize width relative to hotspot size. Generally, a narrower nanowire is more appropriate but can also lead to higher dark counts.
Superconducting bandgap (Δ)	Impacts spectral cut-off; smaller gaps shift sensitivity to longer wavelengths.	Select or design materials with a smaller superconducting bandgap to achieve mid-IR cut-off wavelengths.
Quasi-particle multiplication efficiency (ζ)	Defines efficiency of energy transfer and hotspot formation during photon absorption.	Enhance ζ through material engineering for better quasi-particle multiplication.
Electron diffusivity (D)	Impacts hotspot containment and duration. Lower diffusivity helps localize energy in a smaller region.	Reduce D through material optimization to prolong and localize the hotspot for mid-IR photons.
Electron thermalization time (τ_{th})	Determines hotspot duration and heat dissipation rate.	Engineer material properties to optimize τ_{th} for sustained hotspot duration.
Density of States (N_0)	Affects quasi-particle generation and thermalization.	Mid-IR photons have lower energy compared to visible or near-IR photons, making efficient quasi-particle generation critical. By engineering N_0 to maximize the number of available states near the Fermi energy, the detector can respond more effectively to these low-energy photons.
Superconducting Strip Thickness (d)	Influences hotspot diameter and photon absorption efficiency.	Reducing the thickness can improve mid-IR detection by increasing the energy deposited per unit area.

104 nm-wide nanowires. This study demonstrated that implementing a superconducting nanowire avalanche photodetector (SNAP) configuration significantly enhanced the SNR, approximately by a factor corresponding to the number of parallel nanowires. In the spectral range of 1.3–3.5 μm, the SDE of the parallel-wire SNSPD decreased by a factor of 30, whereas the meander-shaped SNSPD exhibited a three-orders-of-magnitude drop. However, at 3.5 μm, the parallel-wire SNSPD maintained a SDE that was ten times higher [130]. A subsequent study showcased efficient single-photon detection using ultranarrow SNSPDs featuring 20 nm and 30 nm wide NbN nanowires operating at 1550 nm. The 30 nm wide SNSPDs exhibited superior responsiveness to 1550 nm photons and demonstrated improved robustness against constrictions compared to earlier designs. In contrast, the SNR of the 20 nm wide SNSPDs was significantly lower, prompting their redesign into a SNAP configuration to enable compatibility with standard readout circuitry [131]. In a follow-up study researchers incorporated improvements in the nanofabrication process, and a 40 nm wide NbN parallel wire SNSPD demonstrated single photon sensitivity at 10.6 μm [132]. A later study reported a 30 nm wide NbN SNSPD capable of detecting up to 5 μm photons with an efficiency of approximately 2% [133]. However, none of the studies mentioned above achieved saturated IDE behavior for the mid-IR range. Subsequent optimizations in the superconducting film deposition process, including the reduction of film thickness to 6.5 nm and nanowire width to 40 nm, led to the demonstration of a unity IDE at 3 μm and 80% IDE at 4 μm for NbTiN SNSPDs [134]. This progress was further advanced by another study involving 5 nm thick NbTiN SNSPDs, which showcased unity IDE up to 3.5 μm [135].

(2)–(6) Modifying standard superconducting materials to lower their superconducting gap energy, or utilizing low-gap superconductors, can substantially increase the number of broken Cooper pairs (and quasi-particles) generated for a given photon energy absorbed by the nanowire. This approach enhances sensitivity to longer-wavelength photons. However, lowering the gap energy also decreases the critical temperature, requiring the use of advanced cryogenic systems, such as dilution refrigerators or adsorption cryocoolers, to cool the detectors to the temperatures necessary for achieving saturated performance. Low-gap superconductors such as NbSi [136], WSi [137], TaN [138] and MoSi [139] have been employed in SNSPDs, demonstrating higher sensitivity compared to standard Nb-based SNSPDs at a given photon energy. For instance, a 30 nm wide MoSi SNSPD exhibited a saturated IDE up to 4 μm [139]. Additionally, amorphous materials like NbSi, WSi and MoSi, are believed to exhibit extreme structural homogeneity. The absence of grain boundaries in amorphous materials could confer advantages compared to the granular structure found in Nb-based superconductors [140]. Amorphous materials are of particular interest for integration with waveguides, mainly because they can be deposited at low temperature, and their fabrication tolerance may lead to better yields. These are a category of superconducting materials that lack the long-

range order of crystalline and polycrystalline materials [141]. As a result of this, such materials have enhanced superconducting properties but are only structurally stable at very low temperatures <20 K [142]. A clear advantage is that amorphous materials do not require matching to a substrate lattice structure [143] and can be deposited as high-quality films at low temperatures. This results in high fabrication yields and good compatibility with other components of integrated photonic circuits [144]. However, compared to NbN or NbTiN, amorphous superconductors have lower critical temperature and lower band gap, leading to more complicated cooling requirements but much better detection efficiency at longer wavelengths [142].

WSi and MoSi are most commonly used amorphous materials, with SNSPDs fabricated by co-sputtering either Mo or W and Si on a substrate followed by sputtering of an Si overlayer to prevent oxidation during device fabrication [145]. A WSi-based SNSPD has been reported with a timing jitter of 4.8 ps, which is the lowest for any amorphous material [146]. Timing jitter is typically higher in SNSPDs based on amorphous materials compared to those using NbN because of the lower carrier density and correspondingly lower critical current, leading to a lower SNR [147]. MoSi has a similar band gap to WSi, but a critical temperature >4 K even as a thin film [142]. Greater than 98% SDE at telecommunications wavelengths has been achieved with a MoSi SNSPD augmented with distributed Bragg reflectors, which is comparable to the best SDE achieved with any other material [148]. This suggests it is an ideal material choice for high-performance SNSPDs operating with typical commercial cryogenic systems [142]. MoGe can be used to fabricate SNSPDs using a similar process to that followed with WSi [145]. These detectors have similar SDE to those based on WSi but a slightly higher critical temperature, allowing them to operate in closed-cycle cryocoolers at temperatures around 2.5 K [147].

Alternatively, the conventional superconductor NbN can be engineered by tuning the film's stoichiometry to reduce its nitrogen content, resulting in γ-Nb_4N_3 with a tetragonal phase and a lower superconducting gap energy. By thinning the film to 5 nm and reducing the nanowire width to 42 nm, photon sensitivity improved, reaching near unity IDE at 4.8 μm [149]. However, despite efforts to lower the critical temperature to 3.5 K, the expected extension of the cut-off wavelength (the longest wavelength at which photons can be detected with near unity IDE) 10 μm was not achieved, primarily due to fabrication imperfections [150].

Engineering a superconducting material to reduce the density of states at the Fermi level, or equivalently, decreasing the free carrier density, leads to a distribution of photon-deposited energy among fewer quasi-particles within a given volume. At the same time, increasing the thermal impedance along the nanowire's length effectively localizes the deposited energy. This dual modification elevates the effective temperature and energy of each quasi-particle, which facilitates the suppression of superconductivity and enhances energy sensitivity. Importantly, this approach obviates the need for a reduced cross-section area, allowing for the fabrication of high-yield and high-quality SNSPDs. In the case of WSi, reducing the free carrier density was accomplished by tuning the stoichiometry to introduce more Si content, thereby increasing the thin film resistivity. This adjustment did not significantly affect the critical temperature, enabling the operation of various composition SNSPDs at a nearly fixed temperature. The results demonstrated saturated IDE at 9.9 μm achieved with a single 10 μm long and 50 nm wide nanowire [151], and up to 7.4 μm for a large active-area meander-shaped SNSPD [152]. The meander shape is more sensitive to fabrication imperfections, with a higher probability of suffering from constrictions in bends and along the nanowire length, thus having a reduced ability to saturate. Most recently, significant engineering advancements in WSi SNSPDs were made by employing a reduced cross-sectional area, a low superconducting gap energy and reduced density of states, leading to enhanced sensitivity and unity IDE up to 29 μm for the first time [153].

Alternative superconducting material solutions not specific to mid-IR applications are also being explored. For instance, hybridized SNSPDs made from a combination of materials with complimentary properties should allow for greater tunability of material properties and device performance than is possible with single materials. An example of this is a detector with a WSi thin film layered on top of a NbN thin film. Compared to a typical device made with either single material, this yields an improved switching current, timing jitter, and QE [154].

Commercial cryocoolers capable of reaching the low temperatures required by most of these superconductors, are bulky, costly, and run on rare and expensive refrigerants. As such, they are impractical for many applications. For some less demanding applications, it would be desirable to develop high-temperature SNSPDs that do not have such complicated cooling requirements [155]. MgB_2 has a bulk critical temperature of 39 K and has been used to fabricate SNSPDs with high count rate and an operating temperature around 10 K [156]. Unfortunately, all reported detectors based on this material have shown poor internal detection efficiency because of the large band gap and short thermal relaxation time [145]. Cuprate superconductors have recorded high critical temperatures, but it is very difficult to fabricate a high-quality nanowire from a cuprate thin film because they degrade rapidly when processed [157]. Despite these difficulties, SNSPDs have been fabricated from $Bi_2Sr_2CaCu_2O_{8+\delta}$ (BSCCO) and $La_{2-x}Sr_xCuO_4$ (LSCO), showing single-photon sensitivity at temperatures as high as 25 K [155].

4.4. Fiber-to-chip light coupling

One of the main challenges in achieving high SDE for waveguide-integrated SNSPDs, when photons are delivered via an optical fiber, lies at the fiber-to-waveguide coupling interface. Efficiently coupling light from an optical fiber, which typically has a modal area of a few square microns, to an integrated waveguide with a much smaller, sub-micron modal area is a complex task, and it becomes even more challenging at cryogenic temperatures. The most common approaches

to address this include butt coupling or the use of grating couplers. First reported by Hunsperger and Lee in 1976 [158], butt coupling has been the preferred method for coupling light in or out fiber to photonic circuits given its simplicity and effectiveness in implementation. Theoretically, almost 90% coupling is possible to the waveguide, however, in practice, coupling efficiencies are low because even slight misalignment in the direction perpendicular to the fiber can lead to significant coupling loss [159].

On the other hand, grating couplers are essentially diffraction gratings etched into the photonic layer guiding light to the waveguide with an SNSPD, with a pitch chosen to diffract the desired detection center-wavelength to/from the waveguide from/to free space, typically near normal to the plane of the chip. The area of the diffraction grating is typically chosen to match the modal area of the optical fiber, and when the light is incident from the fiber at a small angle, it is diffracted into the waveguide mode that propagates the signal to the superconducting nanowire. Grating couplers are compatible with fiber arrays and can have insertion losses below 3 dB if carefully designed and manufactured [160]. The out-of-plane geometry, though useful for automated screening of optical circuits on a wafer scale, is not ideal for high-performance packaging.

To overcome limitations of butt and grating couplers, Wolff *et al* designed a 3D polymer coupling structure that could be directly laser written. Such polymeric coupler allowed for light coupling over a broadband wavelength range, and they reported waveguide-integrated SNSPDs with system detection efficiencies ranging from 22% to 73% over a broad wavelength range from 532 nm to 1640 nm [161]. The polymer coupler enables total internal reflection across a broad transmission bandwidth, making it possible to couple light over such a broad range. Using similar 3D polymer couplers, Häußler *et al* reported a 64-channel SNSPDs array that could be addressed vertically using 64-channel optical fiber array (see figures 7(a)–(d)) [162]. The efficiency of coupled devices ranged from 20% to 30%.

Photonic wire bonding refers to an automated means of writing 3D polymer waveguides that connect fiber facets to either cleaved edges at the terminus of the waveguides, or to surface tapered waveguides that end within less than 100 μms of the chip facet (see figures 7(b) and 6(e)) [163]. The waveguides in this case are created in a negative tone liquid photoresist through a process called two-photon polymerization using a high-numerical aperture pulsed laser beam. Only low-resolution alignment of a fiber ribbon array (containing up to 32 fibers) to the chip facet on a sub mount is required to achieve insertion losses between 1 and 2 dB [164], as the precise alignment is controlled by the laser beam control algorithm.

In recent years, the use of microlens in conjunction with grating coupler architecture has shown a strong possibility of overcoming the limitations of vertical coupling [165]. Additional support structures like plasmonic nanostructures [23, 166, 167], or angled reflectors for efficient coupling have also shown improved coupling with light [168]. Other interesting ideas are also being explored. For example, in a recent report, Dai *et al* fabricated a complete SNSPD along with contacts on top of a fiber bonded to a silica wafer and could achieve a SDE of about 41%, which is appreciable considering the first attempt [169]. In another report, Shainline *et al* reported a spot-size converter comprising a silicon-based inverse taper waveguide and a large silica core. Using such a design they reduced the light coupling loss to less than 2 dB. In [54], Shainline *et al* proposed another innovative cryogenic-compatible scheme for light coupling with grating couplers. The packaging for fiber alignment consisted of a pedestal to align the fiber at an angle and a collar to hold the fiber in place (see figure 7(f)) [54]. Both the pedestal and the collar were made of SU8.

So far, we have discussed different ways in which an SNSPD can be fabricated directly on top of different kinds of waveguide materials. However, there may be cases where the fabrication of an SNSPD is not compatible with the fabrication of other components of the PICs. For those cases, researchers have been developing pick-and-place membrane transfer technologies. In the next sub-section, we briefly cover some of the developments in the pick-and-place membrane transfer technology.

4.5. Pick-and-place membrane transfer technology

In recent years, researchers have been developing pick-and-place membrane transfer technology for direct integration of SNSPD on top of waveguides [170–172]. Membrane transfer is a relatively new technique for the transfer of optical components for flexible hybrid on-chip integration [173, 174]. In this scheme, the device is fabricated on an arbitrary substrate containing a thin-film, which can be mechanically detached from the substrate to form a membrane and placed on the photonic substrate of interest. For SNSPDs, this transfer technique was first reported by Najafi *et al* in [170]. They fabricated an SNSPD on top of a silicon nitride thin film on a SOI substrate. To create a membrane, they formed trenches using reactive ion etching and later removed the remaining silicon using isotropic etching. The membrane was later detached from the substrate using ultrasonication and transferred on top of the waveguide using PDMS. One of the primary advantages of this scheme is that the device can be optimized and characterized on a different substrate, simplifying the fabrication flow and it can be transferred to an arbitrary PIC. Moreover, with this approach, the devices can be screened for high performance and the best SNSPDs can be selected for transfer, improving the overall yield and uniformity in the final integrated platform. In a recent report, Chen *et al* used transfer printing to mechanically stack two SNSPDs on top of each other [172].

4.6. PNR in waveguide-integrated SNSPDs

Most of the PNR demonstrations have been realized for free-space or fiber coupled SNSPDs, with very few demonstrations of waveguide-integrated PNR SNSPDs. The first demonstration of waveguide-integrated PNR SNSPD used

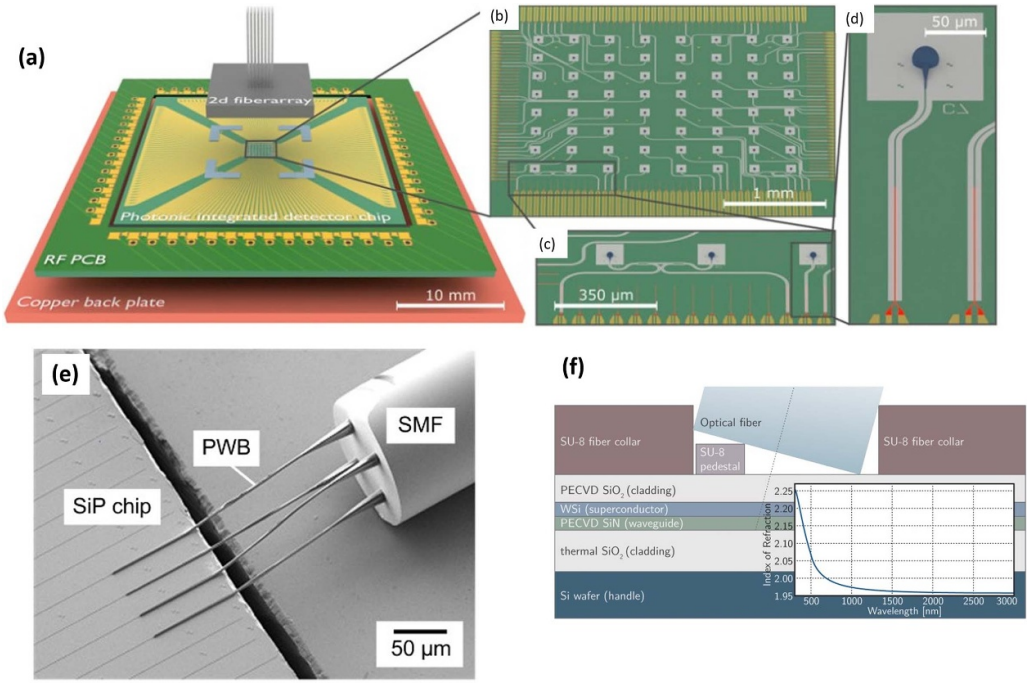

Figure 7. Different schemes for fiber-to-chip light coupling for waveguide-integrated SNSPDs. (a) A 3D schematic of a 64-channel waveguide-integrated SNSPDs chip aligned to a fiber array and mounted on a copper plate. (b)–(d) Shows a magnified view of the chip. The blue blob region shows the 3D light coupler from the fiber array to the waveguide. Figures 7(a)–(d) has been reprinted from [162], with the permission of AIP Publishing. (e) A 3D schematic showing the concept of photonic wire bonding for coupling a multi-core fiber to waveguides. Reproduced from [163]. CC BY 4.0. (f) A 3D schematic showing light coupling of a fiber to a waveguide using an SU-8 pedestal to align the fiber at a small angle relative to the waveguide. Reproduced from [54]. CC BY 4.0.

NbN nanowires patterned atop a GaAs ridge waveguide (see figure 8(a)) [175]. They connected four superconducting nanowires in series with a parallel resistor connected to each of the nanowires and were capable of resolving up to 4 photons. In this scheme, each SNSPD is biased near its critical current, and absorption of a photon disrupts the superconductivity in one nanowire leading to an increase in the nanowire resistance followed by diversion of current to the parallel resistor. As photon number increases from 1 to 4, subsequent nanowires become resistive diverting the current to parallel resistors, increasing the amplitude of the recorded voltage pulses (For more details see figures 8(b) and (c)). Using similar scheme Mattioli *et al* could resolve up to 24 photons, but the device was not waveguide-integrated. In another report, Gaggero *et al* was able to implement amplitude multiplexing with expanded capability to resolve both the photon number and the position of photon absorption event (see figure 8(d)), which can have several applications in photonic quantum technology [176]. The idea was very similar to series connected SNSPDs, except that in this case the resistor's values changed across different pixels, and therefore, by looking at the height of the pulse, the photon absorption position could be assessed. One of the main limitations of any spatially multiplexed PNR SNSPDs is absorption of two or more photons in a single pixel leading to reduced detector fidelity. However, this limitation can be estimated and overcome by having relatively higher number of pixels compared to the number of photons that need to be detected [38].

One of the most recent efforts demonstrated a waveguide-integrated spatiotemporal multiplexed SNSPD array capable of resolving up to 100 photons as well as their detection positions [27]. figures 9(a)–(f) shows the device architecture where light is coupled to an input grating coupler, and incident photons propagate through the waveguide and are spatially distributed to pixels of incremental length integrated atop the waveguide. The pixels are all connected in series, and a nanosecond-level microwave delay line is embedded between neighboring pixels and each pixel is shunted by an on-chip low-pass filter consisting of on-chip inductor and on-chip resistor. The delay lines allow for temporal multiplexing, while the low-pass filters ensure that high-frequency signals enter the readout circuit allowing the reset of individual pixels separately. Eventually, the pixels at both ends of the bus line are connected to impedance tapers for impedance matching between delay lines and readout electronics. A bias tee is connected to each impedance taper, allowing DC biasing as well as readout of a pair of positive and negative detection pulses from fired pixels, propagating in opposite directions of the bus line. Figure 9(g) shows persistence oscilloscope traces of detection pulses generated from each pixel in the detector. The number of pulses, along with their arrival times, can be used to determine the total absorbed photon number and the positions of fired pixels [27]. They claimed to have achieved an unparalleled dynamic range and PNR fidelity, however, the SDE and resolving fidelities of the detector were not reported.

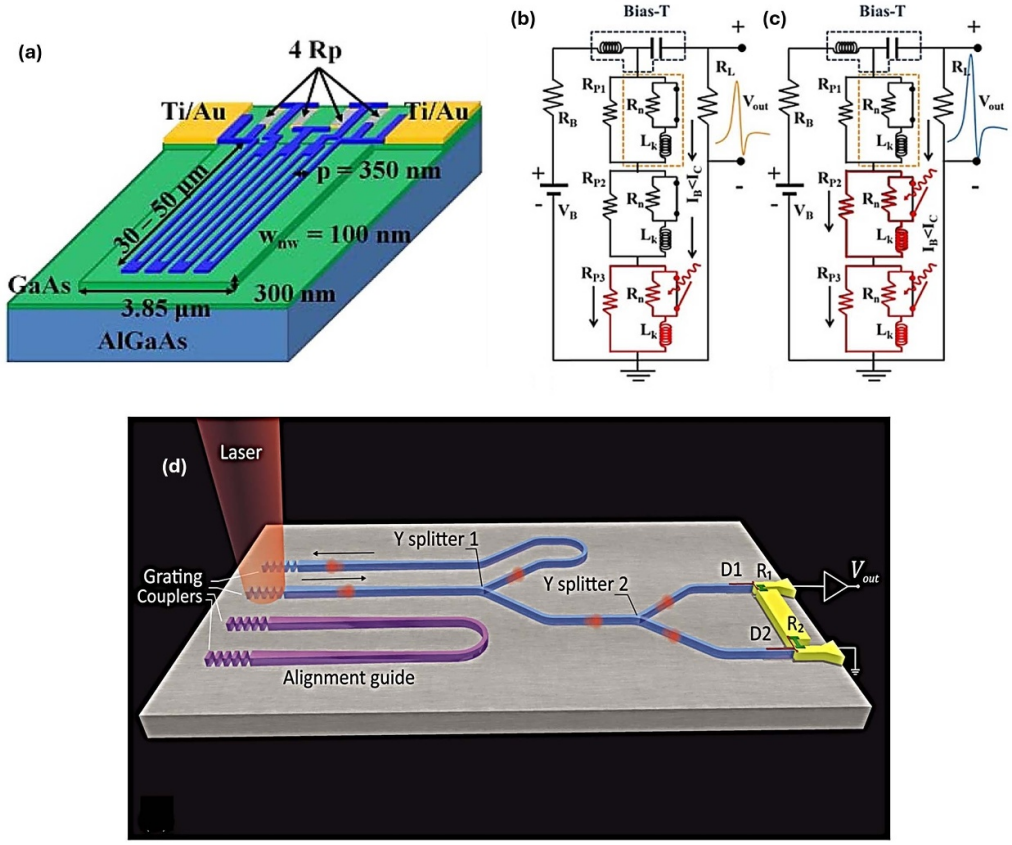

Figure 8. (a) A 3D schematic of a waveguide-integrated PNR SNSPDs atop a GaAs waveguide, capable of resolving up to four photons. The dimensions of the waveguide and nanowires are also shown. R_p represents resistors connected in parallel to the nanowires. (b) A circuit diagram illustrating the working principle of the PNR SNSPD in (a). Each nanowire is modeled as a resistor, R_n, in parallel with a switch and connected in series to an inductor, L_k (highlighted by the orange box in the top pixel). The parallel resistors are denoted as R_{pi}. When a photon is absorbed, the switch opens, introducing R_n into the circuit and causing current to divert and split between the parallel resistor, R_{pi}, and the readout circuit, R_L. (c) The number of pixels that absorbed photons correspond to the number of detected photons. (d) A schematic of waveguide-integrated PNR SNSPDs implementing spatial and amplitude multiplexing to assess both the photon number and the position of photon detection events. The photonic integrated circuit includes grating couplers, 50:50 Y-splitters, two SNSPDs (D_1 and D_2), and parallel resistors R_1 and R_2. Reprinted from [177], with the permission of AIP Publishing. Reproduced from [38]. © IOP Publishing Ltd. All rights reserved. Reproduced from [176]. CC BY 4.0.

Figure 10(a) shows a microscope image of PNR SNSPD on top of a taper waveguide [28, 29, 178]. The device shown in figure 10(a) consisted of four- or five-unit cells and could resolve up to four photons, with near unity SDE (see figure 10(b)). The working mechanism of the device is the same as that used in the series-connected SNSPDs discussed above. The photon number was extrapolated to be directly proportional to the output voltage amplitude of the PNR SNSPDs, as shown in figure 10(c).

More research efforts are focusing on improving PNR SNSPDs while inheriting the exceptional performance metrics of individual SNSPDs. In particular, new schemes are required to achieve high PNR fidelity while maintaining high SDE, alongside high readout fidelity, defined as the overlap in the readout feature from neighboring PNR pixels, and splitting fidelity, defined as the probability of all photons simultaneously switching different pixels.

5. Current applications and perspective for future development

As mentioned in earlier sections, waveguide integration of SNSPDs is expected to significantly enhance their performance by reducing dark counts, improving timing performance, while maintaining near-unity OCDE. This advancement has the potential to impact both classical and quantum technologies. For example, classical technologies such as optical time-domain reflectometry, lifetime imaging, and optical coherence tomography (OCT) benefit from improved SNR and enhanced detector timing characteristics. In contrast, quantum technologies demand even stricter performance in terms of SNR, detector timing, and extremely low timing jitter. However, a major limitation in many quantum applications is the challenge of scaling up the number of detectors and efficiently managing their readout.

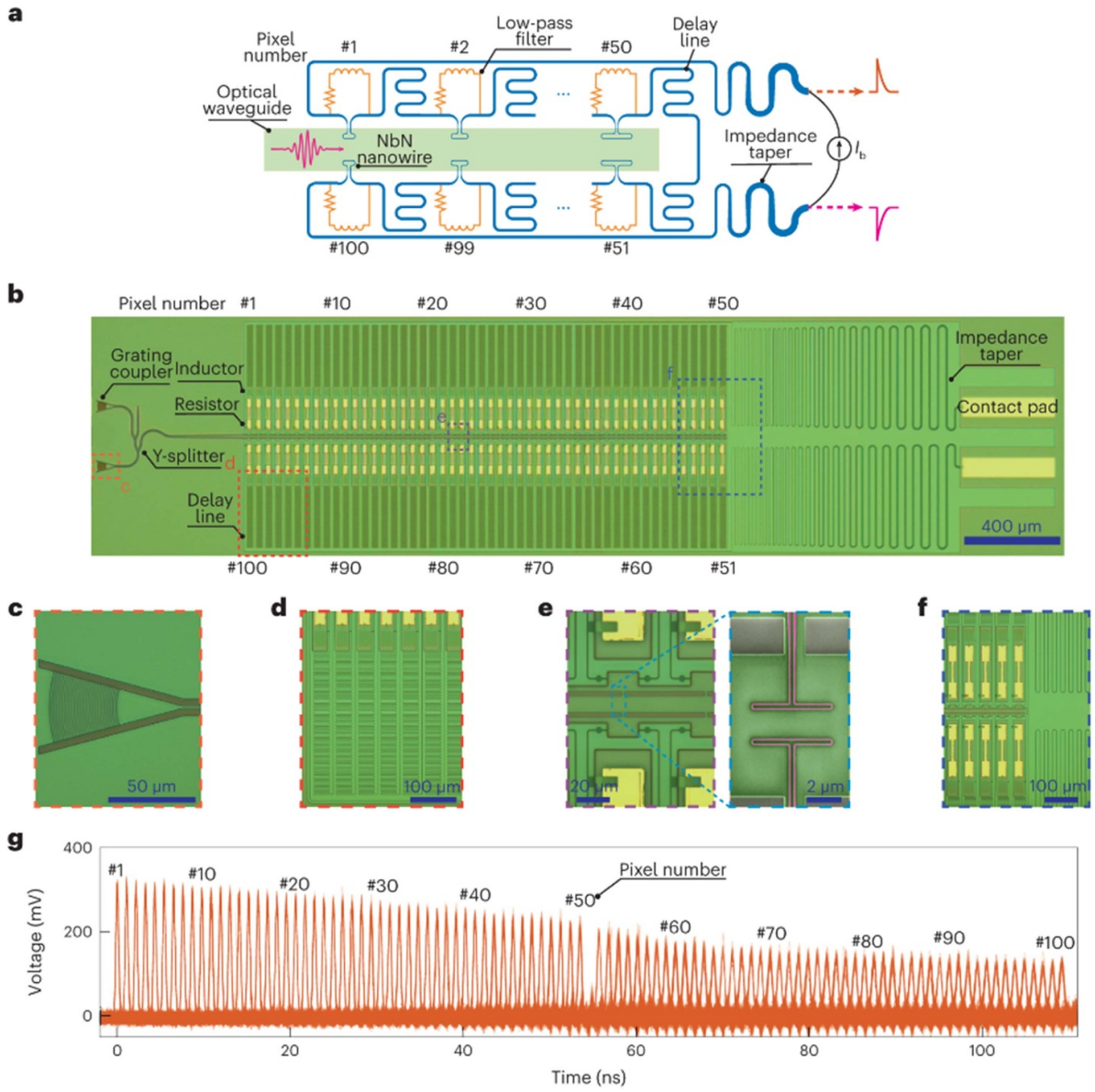

Figure 9. Architecture and operational principle of a waveguide-integrated 100 pixel quasi-PNR spatiotemporal multiplexed SNSPD array: (a) Schematic of the SNSPD array: it consists of NbN pixels of incremental length atop an optical waveguide with delay lines and impedance tapers for the high-frequency bus line (blue), as well as low-frequency reset loops made of inductors and resistors (orange). Current biasing and readout are done at both ends of the bus line, allowing simultaneous readout of positive and negative detection pulses (red). (b) Optical micrograph image of the device showing optical and electrical components, the highlighted boxes show zoomed-in parts: (c) Grating coupler for light coupling, (d) Microwave delay line, (e) Nanowire detector with its electrical leads passing through waveguide bridges, (f) Resistors and part of the inductors creating the on-chip LR low-pass filters and part of the impedance tapers. (g) Persistence oscilloscope traces of detection pulses generated from each pixel in the array. The number of pulses combined with their arrival time can be used to extract both the total detected photon number and the position of fired pixels. Reproduced with permission from [27].

In this section, we provide our insights on the current challenges associated with using waveguide-integrated SNSPD across different applications and highlight potential, unexplored opportunities. We also expand on key technological advancements that are either on the horizon or are necessary to enhance the appeal of waveguide-integrated SNSPDs.

5.1. Optically-enabled quantum computing

All-optical quantum computing can be realized using either continuous-variable (CV) or discrete-variable (DV) computational models. Both models utilize single photons as quantum information carriers but differ in how quantum states are encoded and manipulated. The DV model represents quantum

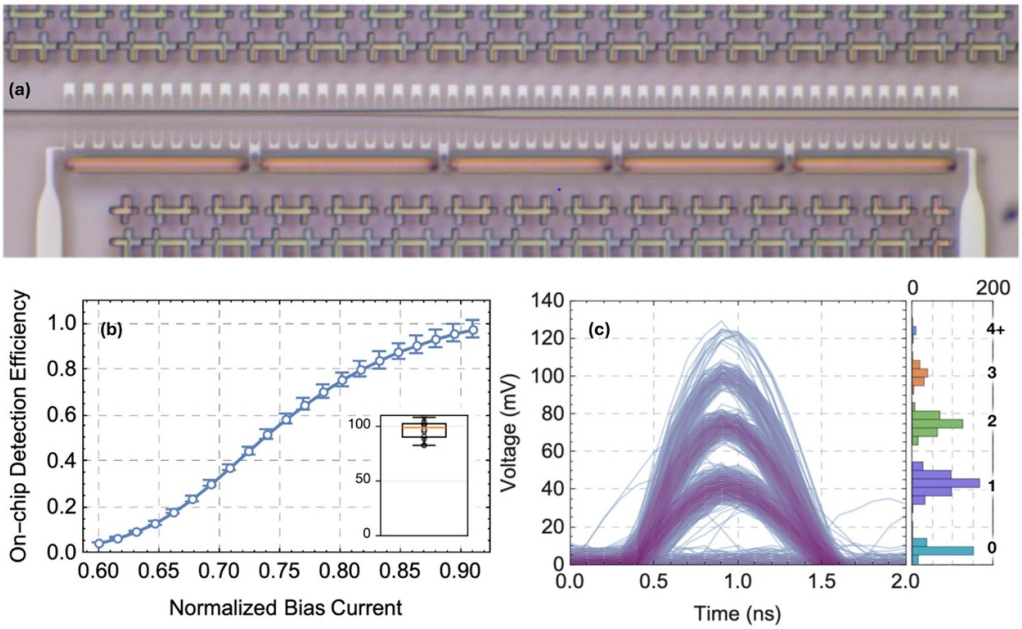

Figure 10. (a) An optical micrograph image of PNR SNSPDs integrated on a silicon nitride waveguide. The device consists of five-unit cells with each unit cell formed by a set of series nanowires, each connected to a parallel resistor. (b) On-chip detection efficiency as a function of normalized bias current. Inset- the average on-chip detection efficiency across 6 different PNR devices biased at ∼0.9 I_{sw} is 96.3 ± 3.9%. (c) Persistence oscilloscope curves showing voltage amplitude as a function of photon number. Reproduced with permission from [29].

states with discrete photon numbers, while the CV model encodes states in continuous parameters, such as the quadrature amplitudes of the electromagnetic field. Regardless of the model, single-photon detectors play a pivotal role in enabling scalable quantum computation.

In 2001, Knill, Laflamme and Milburn proposed the KLM scheme, setting out the theoretical feasibility of universal DV quantum computing using only single-photon sources, linear optical components, and single-photon detectors [179]. This scheme relies on feedback from single-photon detectors for implementing non-deterministic two-qubit gates.

Similarly, the CV approach also relies heavily on discrete-photon detection, particularly in the fault-tolerant Gottesman–Knill–Preskill (GKP) scheme, which encodes qubits in complex nonclassical states with high average photon numbers [180]. This scheme uses linear optical operations, squeezing, homodyne detection, PNR detection and nonlinear mode coupling for the preparation of the encoded states. The creation and manipulation of GKP states are highly dependent on discrete-photon detectors with high SDE, low dark count rates, and PNR capabilities. These requirements align well with the performance characteristics of waveguide-integrated SNSPDs [181].

SNSPDs are essential not only for all-optical quantum computing protocols, but also for other quantum computing platforms that encode and manipulate quantum information using both electronic spin and photonic degrees of freedom [182, 183]. For example, the integration of spin qubits with photonic circuits enables efficient photon routing, high-fidelity readout, and entanglement generation [158]. A similar approach employs color centers in silicon as spin qubits embedded in photonic circuits for fault-tolerant scalable quantum computing [184]. In these applications the SNSPDs are often used to perform parity measurements on multi-qubit states.

All photonically-enabled fault-tolerant quantum computing (FTQC) applications manifestly require that SNSPDs be densely integrated on photonic-chip platforms, owing to its need for manipulating millions of distinct photonic qubits. Photons on chip are routed via lithographically defined waveguides, and the most advanced photonic chip fabrication capabilities currently form these waveguides in silicon or silicon nitride, both of which are highly transparent in the near-infrared. FTQC architectures vary, but all will ultimately require not only SNSPDs, but also non-classical sources of radiation, switching/phase controlling networks. In this application, the area on the chip occupied by each distinct detector must be minimized, especially as they need to be housed in a cryostat. The sensitive detectors need to be isolated from stray light at the single-photon level, requiring on chip attenuation for out of band photons, filtering and shielding from scattered photons or photons generated by other on-chip mechanisms such as luminescence.

Despite their advantages, waveguide-integrated SNSPDs face challenges, particularly in achieving high-fidelity PNR capabilities and expanding their dynamic range. Addressing these limitations is critical for advancing their utility in quantum computing and other photonic application.

5.2. QKD

Classical encryption relies on the computational difficulty of key decryption, which quantum computers threaten to compromise. One alternative approach is to share encryption keys

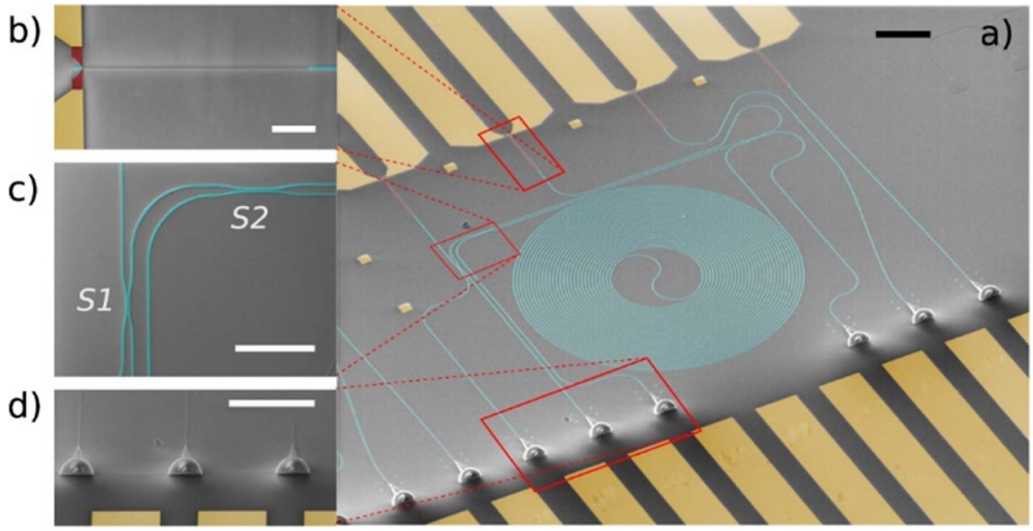

Figure 11. False color SEM images of the receiver chip: (a) the photonic circuit is cyan colored while the electrical pads are yellow colored. The scale bar corresponds to 100 μm. (b) One NbTiN-based SNSPD, red colored, atop a waveguide. The scale bar corresponds to 20 μm. (c) The input directional coupler (S1) splits incident light between an SNSPD and a Mach–Zehnder interferometer (MZI), and the length of the directional coupler (S2) is adjusted such that the power in both arms of the MZI is approximately equal. The scale bar corresponds to 50 μm. (d) The 3D polymer couplers allow for in and out-of-plane light coupling between the chip and a fiber array above the chip. Reproduced from [192]. CC BY 4.0.

using protocols that take advantage of quantum mechanics, known as QKD. Various protocols have been developed and implemented for both discrete variable QKD (DV-QKD) and continuous variable QKD (CV-QKD) [185], leading to the commercialization of QKD systems [186, 187]. Its implementation is facilitated by leveraging the well-established low-loss, high-speed infrastructure of classical communication, particularly in the infrared telecom range, thereby enhancing its feasibility and potential for seamless adoption. For recent comprehensive reviews on the QKD field, refer to [5, 185, 188–190].

A QKD system facilitates the generation, distribution, and reception of a confidential key between two authenticated distant parties, which is subsequently used to encrypt and decrypt information. Thus, the key components of QKD systems are transmitter(s) (also referred to as sources), which generate quantum photonic states, low-loss optical channels over which the photonic states are distributed, and receiver(s) (also referred to as detectors), which process the delivered photonic states.

The performance of a practical QKD system is typically characterized by key performance metrics such as the maximum achievable secret key rate, over a given quantum channel length, the QBER, and the system clock rate. These parameters collectively determine the system's ability to securely transmit information. While the secret key rate reflects the rate of secure key generation, the QBER measures error susceptibility due to noise, imperfections, or eavesdropping attempts. The clock rate defines the operational speed, influencing overall throughput. Optimizing these metrics is crucial for scaling QKD systems for real-world deployment.

Overall, SNSPDs are considered one of the most promising candidates for DV-QKD receivers due to their near-unity SDE, sub-picosecond timing jitter, short dead time, and high-fidelity photon number resolving capability. Koziy *et al* compared two of the most promising single photon detector candidates, i.e. SPAD and SNSPD [191]. They concluded that the choice between SPADSs and SNSPDs depends on the specific requirements of the quantum communication system. For short-distance applications with fewer channels, SPADs may suffice. However, for complex networks requiring high sensitivity and low noise, such as star topology configurations, SNSPDs provide the necessary performance despite their higher operational demands [191].

PICs hold great promise for the miniaturization, scaling up, and cost-effective mass production of practical chip-based QKD systems. Below, we review previously reported results on integrated QKD systems enabled by PICs, particularly those in which the transmitters or receivers utilizing waveguide-integrated SNSPDs. Integrated receivers will provide enhanced performance metrics through the high SDE and low timing jitter of SNSPDs, enabling higher secret key rates through techniques such as wavelength-division multiplexing or parallel channels and potentially lower QBER.

In 2021, the first fully integrated photonic receiver with SNSPDs was demonstrated on a silicon nitride platform, eliminating the need for a fiber coupling interface between the measurement setup and the detectors. The waveguide-integrated SNSPDs allowed a dead time of 20 ns and a dark count rate below 20 Hz. The receiver chip, shown in figure 11, is suitable for multiple time-based protocols. As a proof of principle, a time-bin QKD protocol with one decoy

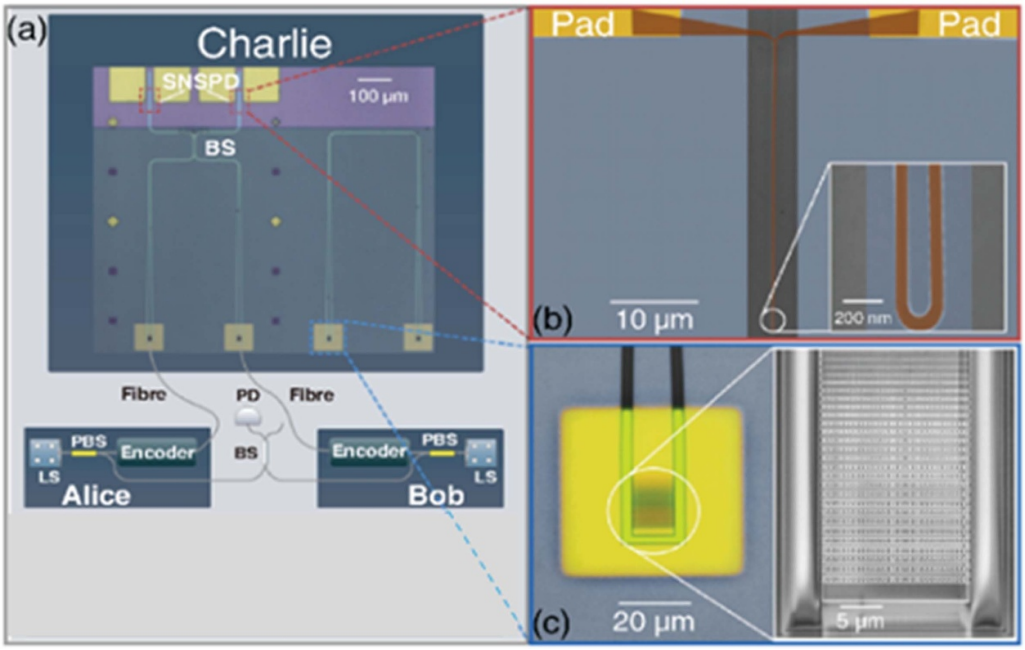

Figure 12. Integrated chip of the relay server and experimental setup for the MDI-QKD protocol. (a) Schematic of the experimental setup. Alice and Bob generate time-bin qubits using two independent lasers (LS) and encode the information into weak-coherent optical pulses using an encoder module. The qubits are sent to Charlie by fibers and are coupled into the integrated chip of the relay server. The chip contains a beam splitter (BS) and two SNSPDs for BSM. (b) False color SEM image of NbN-based SNSPD atop a silicon waveguide and two electrical pads (c) Optical micrograph and SEM image of high-efficiency photonic crystal grating coupler with a back-reflected mirror used for light coupling from the fiber array to the chip. Reproduced from [193]. CC BY 4.0.

state at a wavelength of 1530 nm was implemented at a clock rate of 2.6 GHz. This achieved a secret key rate of 2.5 Mbit s^{-1} at a small attenuation level, where the attenuation level simulated the transmission distance [192]. Later, a time-multiplexed measurement-device-independent QKD (MDI-QKD) protocol was implemented using a relay server made of a silicon photonics chip with waveguide-integrated SNSPDs. The relay server chip, shown in figure 12, acts as a central node (Charlie) and performs optimal Bell-state measurements (BSMs) between two independent lasers (Alice and Bob) at a wavelength of 1536 nm. At a clock rate of 125 MHz, the demonstrated MDI-QKD obtains a secret key rate of 6.2 kbit s^{-1} at an attenuation of 24 dB [193].

One strategy for speeding up the data rates of QKD systems is massive parallelization of the quantum communication bandwidth through signal multiplexing. Figure 13 depicts a fully integrated photonic chip with a four-channel wavelength-division demultiplexed QKD receiver in a silicon nitride platform with eight waveguide-integrated SNSPDs. At a clock rate of 3.35 GHz, a secret key rate of 12.17 Mbit s^{-1} at an attenuation of 10 dB was achieved, along with a low detector-induced QBER and negligible crosstalk between the four channels [194].

The state-of-the-art QKD receiver based on waveguide-integrated SNSPDs supports up to 64 channels with a total photon detection rate of up to 1.6 GHz. The waveguide integration enables the inspection of the receiver chip before defining the photonic layer to pre-select the best 64 nanowires, as shown in figure 14. The detectors exhibited a count rate of up to 20 MHz, timing jitter below 120 ps, and DCR below 150 Hz at 3.6 K. The receiver was utilized in a highly parallelized multichannel wavelength-division multiplexed QKD system where each QKD channel uses two SNSPD channels. Due to a high thermal load to the cryostat hosting the receiver, only 18 detection channels were used in the QKD experiment, demonstrating a maximum secret key rate of 13.2 Mbit s^{-1} for 9 wavelength channels and 3.82 kbit s^{-1} for 26.6 dB attenuation [195].

To summarize, as the QKD technology becomes more widely adopted and quantum communication networks grow in complexity, there will be an increasing demand for higher channel counts. This demand will drive the development of multi-source heralding single-photon source modules and associated detector arrays, aligning with advancements in technology for optical quantum computing. In this context, the development of waveguide-integrated SNSPDs is pivotal for advancing QKD transceivers. In party-to-party protocols that do not involve entanglement, an N-channel QKD receiver chip featuring N integrated decoding circuits—each containing a waveguide-integrated SNSPD—would connect to a 1D or 2D fiber ribbon carrying N distinct inputs. For entanglement-based protocols utilizing a central node, the connectivity and decoding configuration on the chip at the central node would differ. Nevertheless, the requirement for multiple waveguide-integrated SNSPDs remains constant, underscoring the critical role of waveguide integration in driving future advancements.

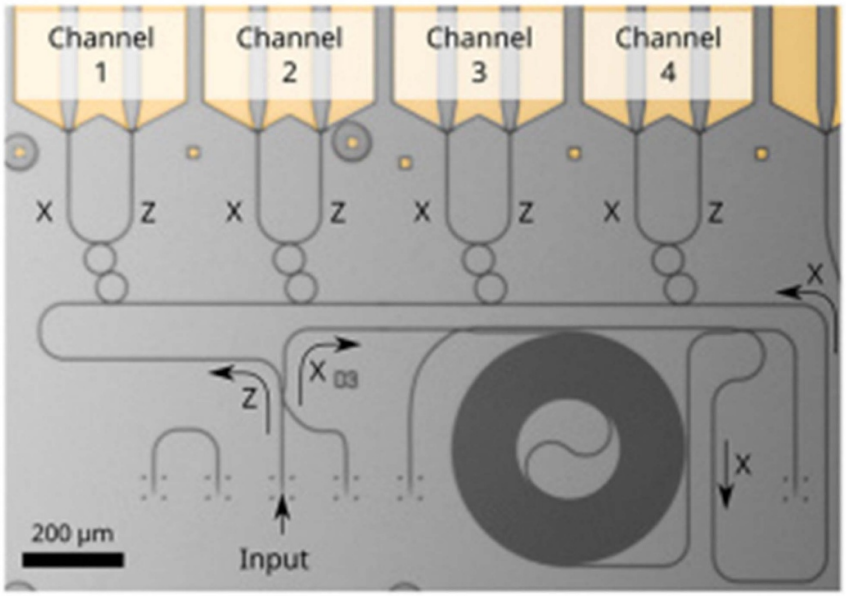

Figure 13. False color optical micrograph of the receiver chip with four-channel wavelength-division demultiplexers. The input light is split through a directional coupler, acting as a passive basis selection splitter. Most incident light is sent directly into the on-chip demultiplexers (Z) and read out by one SNSPD to measure the data bits of the transmitted key. The rest (X) goes through a delay line interferometer, where one arm contains a spiral waveguide delay line. The interferometer output is forwarded to the demultiplexers as well and read out by the second SNSPD. The demultiplexers are made of serially coupled ring resonators. Each channel has 2 NbN-based SNSPDs, and their electrical pads are yellow colored. Light coupling into the chip is achieved through 3D polymer couplers. Reproduced from [194]. CC BY 4.0.

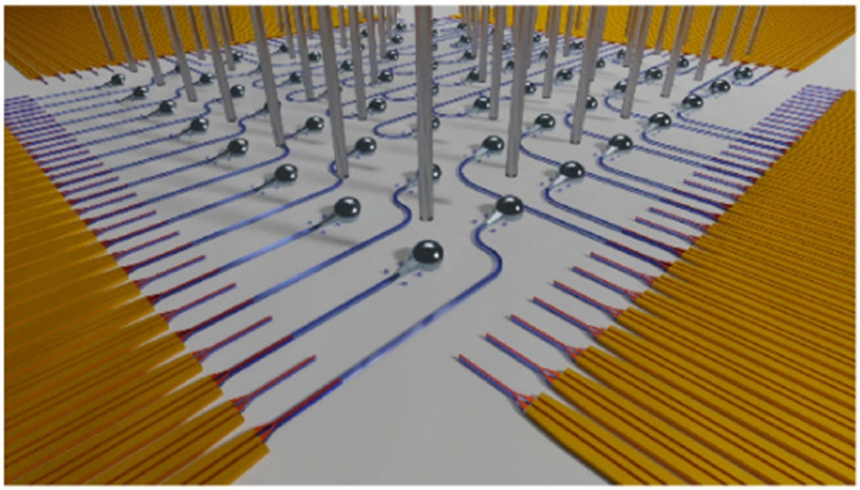

Figure 14. Schematic of a 64-channel 2D fiber array (grey) above the QKD receiver chip. The fiber cores are aligned to 64 3D polymer couplers (glossy) on the chip, coupling light into waveguides (blue) with SNSPDs (red). Only the best 64 SNSPDs are waveguide integrated. Reproduced from [195]. CC BY 4.0.

5.3. Fundamental quantum physics

Waveguide-integrated SNSPDs operate in a controlled and isolated environment, reducing noise and interference from external factors, making them useful to explore new avenues of fundamental quantum physics. For example, SNSPDs with near-unity efficiency with diminishingly small dark counts are a key enabler for fundamental quantum physics studies such as quantum nonlocality, quantum walks, and for the distinction between classical and quantum sources [196]. Similarly, several fundamental questions in quantum physics employ interferometric measurements, where noise can ruin the contrast, especially in cases where strong filtering or post-selection is required [197]. In such cases having an on-chip SNSPD can significantly improve the experimental results.

There are also recent advances in photon number resolving waveguide-integrated SNSPDs, which can have a huge impact on on-chip detection of Fock or NOON states,

which is fundamental to a range of quantum applications and quantum physics experiments. Similarly, low dead time and few ps timing jitter are important for decay dynamics measurements. Given waveguide-integrated SNSPDs can achieve few ps timing jitters while maintaining high efficiency, they can be very useful for resolving fast (superradiant) emissions from quantum light sources, such as quantum dots. Similarly, second-order correlation measurement, which makes the foundation of a range of quantum applications, is strongly affected by the dark count of the detectors [198].

Quantum erasers or quantum delayed choice experiments are another important fundamental experiment where precise spatiotemporal measurements of photons can provide new insights into this relatively complex experiment [199].

Quantum acoustics is another emerging field where SNSPDs have been used to characterize single phononic modes [200, 201]. To detect phononic modes, they were mapped onto photonic states, which are then detected by SNSPDs [200, 201].

5.4. Quantum memories and repeaters

When entangled photon pairs are shared between two remote parties (nodes), the losses in the communication channels restrict the maximum distance at which entanglement can be successfully maintained and utilized. Typically, this distance is around 100 km in fiber-based systems [202]. This limitation poses a serious challenge for applications like QKD (section 5.2) and quantum networks, which require long-distance entanglement distribution. Quantum repeaters are devices designed to extend the range of quantum communication by dividing a long communication channel into shorter segments, thereby reducing the impact of photon loss. They function analogously to classical repeaters, but instead of simply amplifying signals, they use quantum principles to distribute entanglement across long distances [202, 203]. Quantum memories and entanglement swapping are the two most important components of quantum repeaters [204].

The total heralding efficiency of the memory node plays a pivotal role in determining the overall success of quantum communication, especially in the context of Bell state measurements, which are essential for quantum entanglement swapping, teleportation, and other key protocols in quantum networks. Heralding efficiency reflects the probability that a successful detection event will occur when a photon is present, which directly impacts the reliability and scalability of quantum communication systems. One of the most significant contributors to the heralding efficiency of quantum memories is the SDE of the SNSPDs [205]. The dark count rate is another important factor one has to consider when choosing detectors for quantum memory applications. So far, there have been several different schemes for on-chip quantum memories using stand-alone SNSPD systems [205, 206], however, integration of on-chip quantum memory with on-chip SNSPDs has not yet been attempted.

5.5. On-chip single-photon spectroscopy

Single-photon spectroscopy or ultra-low light spectroscopy can have a wide range of applications in fluorescence and medical imaging, astronomical spectroscopy, and long-distance daytime remote sensing. Moreover, a high performance, single-photon detector with the ability to distinguish photon wavelength with extreme precision, low timing jitter, and high speed is ideal for emerging quantum communication protocols such as wavelength division multiplexed quantum communications [207]. The wide spectral range of SNSPDs, along with extremely low dark count makes them an ideal candidate for ultrawideband single-photon spectrophotometers. However, SNSPDs operate in a highly non-linear regime, responding similarly to all colors of light within a specified range and therefore cannot distinguish between different wavelengths of light. While several studies have explored the use of SNSPDs for spectroscopy, given the limited scope of the review, we only discuss cases where waveguide-integrated SNSPDs have been employed for spectroscopy applications.

One way to overcome the binary response of SNSPDs is to use waveguide-integrated SNSPDs, where wavelength filtering/demultiplexing can be achieved through ancillary integrated photonic components before detection of photons by SNSPDs. For example, in stationary-wave integrated Fourier-transform (SWIFT) spectroscopy, SNSPDs can be waveguide-integrated to detect the evanescent field formed by the stationary waves (see figure 15) [208]. The first report of a SWIFT spectroscope based on waveguide-integrated SNSPDs was reported by Cavalier *et al* [209, 210] In a SWIFT spectrometer, the incoming light is split between two waveguides and recombined using a loop waveguide. The SNSPDs lie atop the loop waveguide, and the spectra are distinguished by analyzing the total counts across all SNSPDs atop the waveguide where the stationary wave is formed. The count rate of the SNSPDs depends on their relative position to the stationary wave. SNSPDs at the antinode position give a maximum signal, whereas SNSPDs at node positions give the minimum signal. Because different spectra form different stationary waves, measuring the total counts allows the spectra to distinguish based on reading counts on SNSPDs. To overcome the fabrication limitations of many detectors with individual readouts for high-resolution SWIFT spectrometers, Elshaari *et al* in collaboration with Single-Quantum developed SWIFT spectrometer with slow-RF coplanar waveguide for time-division-multiplexing of single-photon detectors. This architecture allowed the biasing and readout of detectors using a single RF coplanar waveguide [211].

The use of periodic grating structure has long been recognized as an effective way of realizing high resolution spectrometers [213]. The operational principle of grating relies on the phenomenon of diffraction and interference of light.

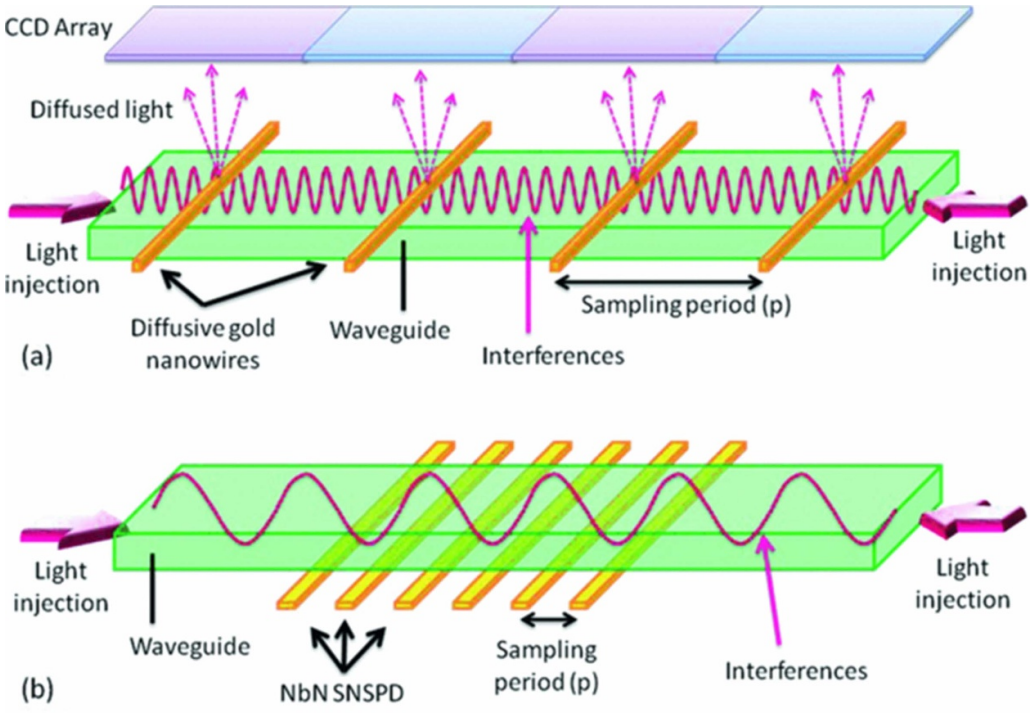

Figure 15. (a) Schematic representation of conventional CCD based SWIFT device. In this scheme, gold nanowires are positioned above the waveguide and diffuse light proportional to the local intensity beneath them, directing the signal toward a CCD array. This approach enables signal probing but is limited by a relatively large sampling period. In contrast, the SWIFT-SNSPD prototype shown in (b) employs on-chip SNSPDs to directly detect a fraction of the localized light within the waveguide. This method significantly improves resolution by using a much finer sampling period, offering enhanced precision and scalability for photonic integration. Reproduced from [212]. CC BY 4.0.

Cheng *et al* demonstrated a broadband single-photon spectroscope based on a single SNSPD integrated into a millimeter-size nanophotonic echelle grating. To read out the SNSPD signal, they implemented a superconducting nanowire delay line with group velocity as low as 0.0073c, where c is the speed of light. Figures 16(a)–(d) shows a 2D schematic of the implemented spectroscope based on echelle grating and an SNSPD. The working principle of device is illustrated in figures 16(e) and (f). The grating is illuminated with a broadband source, where due to diffraction, the light is separated into a spectrum of wavelengths, and they land at different positions on the superconducting nanowire delay line, and depending on the difference in timing arrival the wavelength of light can be assessed [207]. In another report, Zheng *et al* implemented an on-chip spectrometer through the integration of a Rowland grating with a specifically designed SNSPD array in the focusing region of the grating [214]. The specifically designed SNSPD array is coiled in such a way that the filling ratio of nanowires changes spatially, making the absorption in the nanowires a partially varying function. As mentioned, due to diffraction each wavelength lands at a specific position, therefore, by measuring the photon counts across different filling factor SNSPDs, the spectrum of wavelengths could be mathematically reconstructed. Figures 16(g) and (h) respectively show the schematic of a spatially varying coiled SNSPD array integrated with a Rowland grating and the working principle of the spectrometer.

Moreover, in recent years, it has become clear that structural disorder and light scattering, which are generally considered detrimental, can be used to advantage [215, 216]. When coherent light propagates through a highly disordered medium they are scattered several times, and the light forms speckles patterns, due to interference of multiple waves of the same frequency of light but with different amplitudes and phases. The working principle of such devices is based on the analysis of the wavelength-dependent speckle patterns to distinguish closely spaced wavelengths with high spectral resolution. For example, Gupta *et al* could achieve attometer-scale wavelength precision for a speckle-based spectrometer, which they mentioned to have six orders of magnitude better resolution than the commercial state-of-the-art [217]. Using a similar principle, Hartmann *et al* used an on-chip waveguide-integrated SNSPD on a silicon nitride platform, and a controlled disorder medium by etching random air pockets in a high index material (SiN_x) to achieve a spectrometer with 30 pm wavelength resolution.

5.6. *Biomedical imaging*

Recent breakthroughs in multi-pixel waveguide-integrated SNSPDs and on-chip spectroscopy present new unexplored opportunities in biomedical imaging. To date, waveguide-integrated SNSPDs have not delivered concrete results in imaging applications, likely due to readout limitations at the

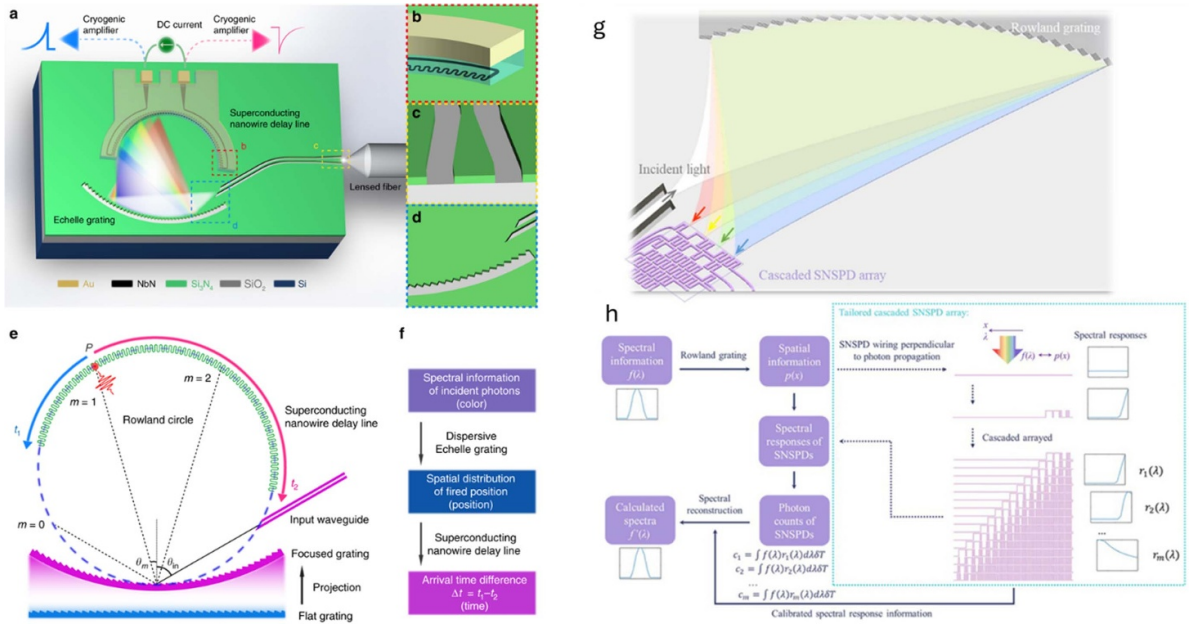

Figure 16. (a)–(d) Illustrate different components within the on-chip single-photon spectrometer. The on-chip focusing echelle grating serves as a wavelength-selective microphotonic element, while the superconducting nanowire delay line operates both as a single-photon detector and as a slow microwave delay line for continuous mapping of dispersed photons. The nanowire is coated with alumina, a high-k dielectric material, and topped with aluminum to form a slow microwave transmission line. (e) Summarizes the working principle of the spectrophotometer. The input waveguide and superconducting nanowire are aligned along the Rowland circle, which internally tangents the focusing grating line. The spatial distribution of incident photons can be calculated using time-tagged single-photon signal or the arrival time difference, as shown in (g) and (h). The photon-counting reconstructive spectrometer combines a Rowland grating and a tailored cascaded SNSPD array for on-chip spectral analysis. The grating spatially disperses light based on wavelength, directing photons to a region with sequentially arranged SNSPDs. Through post processing and spectral reconstruction across wavelengths, high resolution single-photon spectroscopy could be performed. Reproduced from [218]. CC BY 4.0. Reproduced from [214]. CC BY 4.0.

multi-pixel scale. However, future advancements, particularly in the mid-IR regime, could unlock a vast range of applications in this field. In particular, OCT could benefit significantly from SNSPDs, especially in the mid-IR, where reduced scattering improves imaging depth [218]. Mid-IR OCT enables molecular imaging without contrast agents, while on-chip SNSPDs offer seamless integration for hyperspectral imaging, aiding in cancer detection, oxygen saturation monitoring, and surgical guidance [212, 219]. Figure 17 shows an application of SNSPD for enhanced *in-vivo* non-invasive, ultra-deep brain imaging.

Stand-alone SNSPD systems have already shown promise in brain imaging, with improved depth resolution in fluorescence imaging and diffuse correlation spectroscopy (see figure 17) [220, 221]. Clinical trials have already demonstrated their advantages over conventional detectors. Additionally, SNSPDs may enhance brain–machine interfaces by detecting ultraweak neuronal photon emissions.

Other potential applications include photodynamic therapy for cancer treatment via time-resolved singlet oxygen luminescence detection [222–224], and breath analysis [225], a non-invasive diagnostic tool for diseases like cancer and diabetes.

5.7. Artificial intelligence and machine learning (ML)

The compact and scalable nature of waveguide-integrated SNSPD makes them ideal for large-scale classical and quantum photonic circuits, which are crucial for implementing algorithms that could enhance ML tasks. Their high SDE and low jitter can improve the quality of quantum data, which is essential for reliable quantum-enhanced ML [226, 227]. Photonic AI chips that use waveguide-integrated SNSPDs can handle high-throughput data streams while operating with extremely low noise, enabling real-time data analysis and decision-making at discounted energy requirements. There has already been some development in the use of waveguide-integrated SNSPDs for neuromorphic computing, and there are several theoretical schemes, however, so far, there is no concrete step in applying these technologies for the implementation of full-fledged AI or ML algorithms. Quantum computing promises to vastly accelerate AI tasks such as optimization, data analysis, and pattern recognition, which are computationally intensive. In addition, AI and ML have shown immense capabilities in enhancing the single-photon computational imaging capabilities, and in the future, it would be interesting to implement on-chip SNSPDs for imaging in

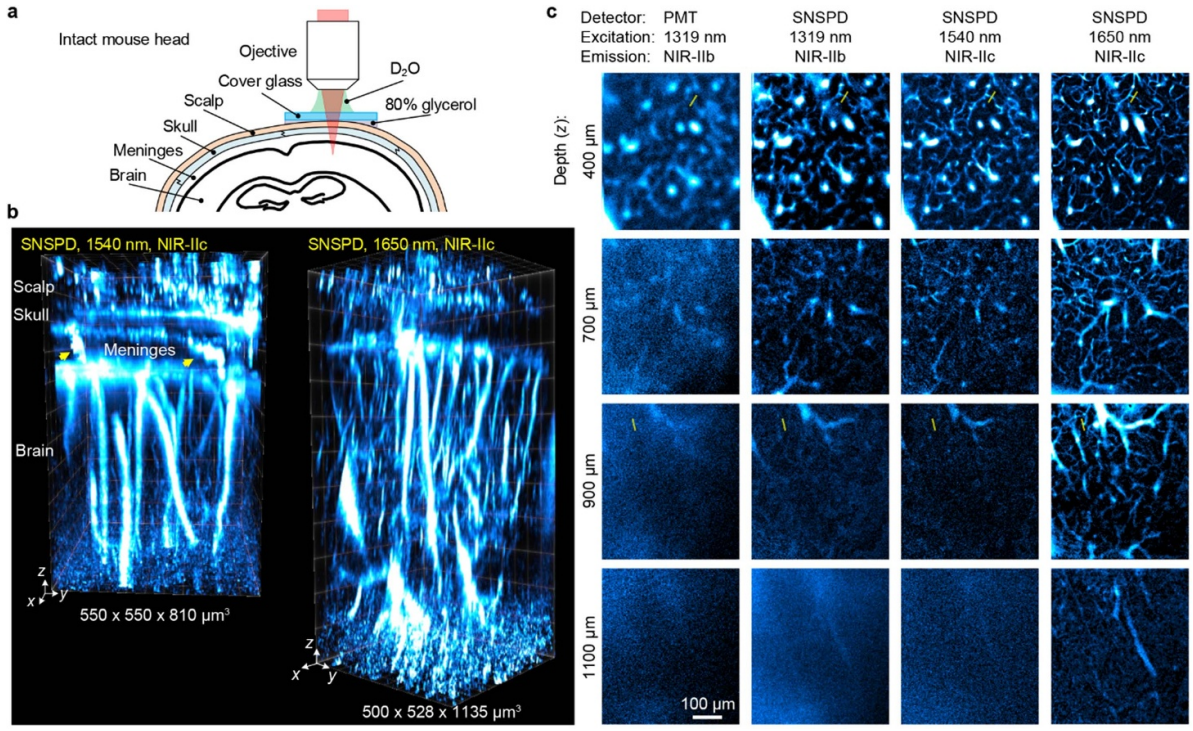

Figure 17. An example of enhanced brain imaging using SNSPDs. (a) Measurement scheme for *in-vivo* imaging of intact mouse brain. (b) Volumetric 3D images of blood vessels in an intact mouse head, visualized through the scalp, skull, meninges, and brain cortex, were captured using a 5 μm z-scan increment. (c) High-resolution confocal images of blood vessels at various depths within an intact mouse head were captured using a PMT or SNSPD in the NIR-IIb (1500–1700 nm) or NIR-IIc (1700–2000 nm) window. It is quite clear that increasing the wavelength improves the depth resolution of applied microscopy. Reproduced from [222], with permission from Springer Nature.

combination with AI processors for images processing. This can be revolutionary for long-distance LiDAR, biomedical imaging, remote sensing, and fluorescence-lifetime imaging microscopy.

5.8. Environmental monitoring

SNSPDs can be a crucial technology for remote atmospheric particle detection and weather forecasting. In photon-based atmospheric radar systems, detecting extremely weak echo signals demands the use of single-photon detectors with high SDE and an exceptionally high SNR. Currently, InGaAs/InP avalanche photodetectors operated in Geiger mode are used for LiDAR based weather prediction/environmental monitoring [228, 229]. However, these detectors suffer from low SDE, high dark count rates, and active/passive gate pulse suppression, which limits the maximum detection range to about 20 km [230]. On the contrary, SNSPDs can detect light with near-unity SDE and negligible dark counts across a wide spectral range, making them extremely useful for long-distance environmental monitoring. Moreover, with the increasing impact of greenhouse gases on the environment, it is becoming imperative to find new ways to monitor these gases in real time. Most of these greenhouse gases have absorption in the mid-IR range and given that SNSPD technology allows for the detection of mid-IR photons at a single photon level, SNSPDs can provide unparalleled real-time information about different greenhouse gases. For example, Zhang *et al* used an SNSPD system with an on-chip integrated lithium niobate micro-ring filter for high-precision spectroscopic measurement of localized spaceborne carbon dioxide (see figure 18) [231]. This kind of system can provide real-time data on almost all kinds of spaceborne greenhouse gases. Additionally, Luo *et al* generated on-chip NOON state for quantum enhanced sensing of temperature and humidity with high precision [232]. In the future, it would be interesting to explore on-chip integration of SNSPDs for a compact quantum-enhanced temperature and humidity sensor for niche applications in environmental monitoring.

Exploring additional avenues for developing mid-IR sensitive SNSPDs with saturated IDE could involve investigating novel thin film deposition techniques that enable the production of highly homogenous films, such as ALD [233], and molecular beam epitaxial growth [234]. Additionally, post-processing defect engineering, achieved by irradiating SNSPDs with helium ions [235, 236], could also be beneficial. While these approaches have been primarily explored in the near-infrared range, further research is essential to assess their effectiveness for lower-energy photons. It should be noted that, thus far, all demonstrated mid-IR SNSPDs have been free space coupled. Potential integrated photonic platforms for this advancement might include silicon, chalcogenide glass, silicon nitride, III–V materials, germanium, and diamond. A recent study tested U-shaped NbTiN nanowires on a SOI

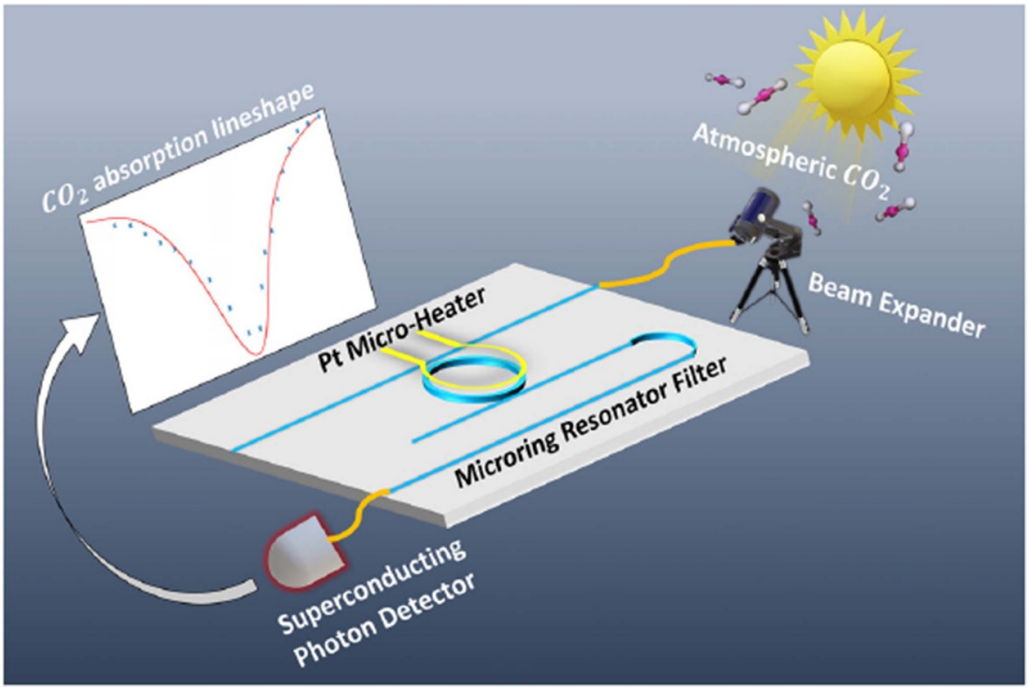

Figure 18. Schematic showing an on-chip micro-ring resonator filter used in combination with an SNSPD for atmospheric CO_2 monitoring. Reprinted from [231], with the permission of AIP Publishing.

platform under flood illumination, demonstrating near-unity IDE up to 3.5 μm [237]. This work demonstrates a material platform that could be used to realize a waveguide-integrated mid-IR SNSPD.

In addition to enhancing energy sensitivity and achieving saturated IDE for mid-IR SNSPDs, addressing the high background count rate (BCR) presents a notable challenge. Reducing the BCR requires incorporating appropriate cold filtering stages along the optical path before the SNSPD, or utilizing on-chip filters to mitigate black-body radiation coupled from the room temperature environment [134]. Successfully achieving this will necessitate careful design considerations for both the cryogenic setup and device packaging.

5.9. Quantum imaging and quantum spectroscopy

While significant progress has been made in enhancing spectroscopy with waveguide-integrated SNSPDs (see section 5.5), the development of multi-pixel imaging arrays remains limited. The development and implementation of readout architecture capable of efficiently interfacing hundreds or thousands of SNSPDs continues to pose a significant challenge. In this regard, there have been some major steps and some interesting and insightful reviews. [238–242] However, most of these works are limited to free-space coupled SNSPDs. In the future, several of these schemes will potentially be reproduced with waveguide-integrated SNSPDs. Recently, Opriov *et al* reported a superconducting nanowire single-photon camera with 400 000 pixels [243]. Note also that there has been considerable interest in integrated photonics for LiDAR systems [244], either for compact beam steering for scanning laser or with the receiver, therefore a waveguide-integrated SNSPD array could be combined with other photonic integrated components for an ultra-compact infrared single-photon LiDAR system.

Interaction-free quantum imaging techniques are another emerging field of quantum imaging, where a target can be imaged without interacting with it [245, 246]. This kind of imaging technique is based on non-invasive imaging, where objects can be observed without the risk of damage or alteration. This is particularly useful in biological research where light-sensitive tissues or fragile structures, like proteins, need to be studied without harm. By minimizing direct contact, interaction-free quantum microscopy preserves the integrity of delicate quantum systems that would otherwise be disrupted by traditional imaging methods. Another benefit of interaction-free quantum imaging is the ability to perform high-precision quantum measurements, especially in quantum computing and quantum information research, where preserving quantum coherence is essential. The method is also highly efficient, requiring fewer photons to produce detailed images. This makes it valuable in fields like astronomy or microscopy, where reduced light exposure can be crucial. Moreover, its potential applications extend to quantum cryptography, where it could be used to detect eavesdrops without directly interacting with the communication stream.

6. Key challenges of WSNSPDs

To summarize, there are several technical challenges that must be systematically addressed to unlock the full potential of WSNSPDs. These challenges can be broadly categorized into

optical coupling, cryogenic electronics, and large-area fabrication consistency, each of which plays a critical role in determining the overall system performance.

Optical coupling: (i) if the application involves the detection of photons generated off-chip, coupled to a WSNSPD array, the primary challenge lies in achieving multi-channel, low-insertion loss coupling between optical fiber arrays and the waveguides with which the superconducting detector elements are integrated. Various approaches involving tapered waveguides to adiabatically adapt the mode areas of the on-chip waveguides and the optical fibers, in either edge- or surface- geometries are being developed, along with arrays of grating couplers. All still face significant challenges to meet the deep sub-dB, polarization insensitive, broadband specifications that many applications will demand. To fully take advantage of these, should they be developed, it will also be desirable to develop WSNSPD structures that show high absorption efficiency for all of the modes launched into the waveguides from different polarizations in the input fiber. (ii) If the photon sources are on-chip, or co-located in a cryostat with the WSNSPD chip, then the biggest challenge is managing any stray 'noise' photons that may be present either in the waveguiding circuit, or in the substrates.

Cryogenic electronics and readout integration: WSNSPDs may require integration with low-noise cryogenic electronics to enable efficient signal readout while maintaining high detection efficiency. One key issue is impedance matching between the superconducting nanowire and the readout circuitry, which affects both timing jitter and noise performance. Although high-impedance cryogenic amplifiers and impedance-matching networks can mitigate this issue, they introduce additional complexity in power dissipation and thermal loading. Future solutions may involve on-chip superconducting amplification and multiplexing architectures, minimizing power dissipation while improving scalability for large-channel systems. Additionally, it would be worthwhile to investigate how developments in on-chip semiconductor cryogenic devices could be adapted to enhance the performance of WSNSPDs.

Fabrication consistency and scalability: fabrication challenges become increasingly critical when scaling up WSNSPD integration. Variability in waveguide patterning, etching non-uniformity, and nanowire deposition inconsistencies can all contribute to performance deviations across large-scale devices. Given that superconducting nanowires operate at bias currents very close to their critical threshold, even minor fabrication-induced non-uniformities can significantly impact the switching current, leading to variations in detection efficiency and timing jitter. Maintaining tight process control is, therefore, essential to ensuring uniform device performance across an integrated system. Additionally, stress-induced defects and process-dependent critical current variations impact the reproducibility of large-scale SNSPD arrays. To overcome these challenges, advancements in deep-UV and electron-beam lithography techniques, combined with ML-based fabrication process control (for example, including image processing), could enhance yield and consistency. Furthermore, the development of monolithic integration approaches could streamline the manufacturing process, reducing reliance on high-precision hybrid integration techniques.

7. Conclusions

In conclusion, waveguide-integrated SNSPDs are expected to be critical for diverse range of quantum and classical applications, because of their compatibility with various photonic platforms and potential scalability. This review highlights the theoretical principles, integration strategies, material developments, and technological innovations driving progress in this field. Advancements in integration schemes and materials have enabled significant improvements in OCDE, timing jitter, and spectral bandwidth, while emerging approaches to circuit design and packaging are addressing practical deployment challenges. Applications in quantum communications, quantum computing, LiDAR, and mid-IR sensing demonstrate the versatility and potential of waveguide-integrated SNSPDs in revolutionizing photonics technologies. Looking forward, continued efforts in material optimization, device engineering, and system-level integration will be crucial for overcoming current limitations and enabling new functionalities. As the demand for scalable and efficient single-photon detectors grows, waveguide-integrated SNSPDs are well-positioned to drive innovation in both research and industry, especially those related to development of quantum technologies.

Data availability statement

No new data were created or analysed in this study.

Acknowledgments

Authors acknowledge the funding from the UK Engineering and Physical Sciences Research Council (EP/T00097X/1, EP/S026428/1) and Science and Technology Facilities Council (ST/T005920/1). AA acknowledges financial support from the SBQMI QuEST fellowship program and NSERC CREATE in Quantum Computing Program (Grant No. 543245).

ORCID iDs

Vidur Raj https://orcid.org/0000-0001-5044-0934
Adan Azem https://orcid.org/0009-0008-8707-6206
Max Patterson https://orcid.org/0009-0004-6628-9887
Robert H Hadfield https://orcid.org/0000-0002-8084-4187

References

[1] Gol'tsman G N, Okunev O, Chulkova G, Lipatov A, Semenov A, Smirnov K, Voronov B, Dzardanov A, Williams C and Sobolewski R 2001 Picosecond superconducting single-photon optical detector *Appl. Phys. Lett.* **79** 705–7

[2] Hadfield R H, Leach J, Fleming F, Paul D J, Tan C H, Ng J S, Henderson R K and Buller G S 2023 Single-photon

detection for long-range imaging and sensing *Optica* **10** 1124–41
[3] Hadfield R H 2020 Superfast photon counting *Nat. Photon.* **14** 201–2
[4] Esmaeil Zadeh I, Chang J, Los J W N, Gyger S, Elshaari A W, Steinhauer S, Dorenbos S N and Zwiller V 2021 Superconducting nanowire single-photon detectors: a perspective on evolution, state-of-the-art, future developments, and applications *Appl. Phys. Lett.* **118** 190502
[5] Zhang C-X, Wu D, Cui P-W, Ma J-C, Wang Y and An J-M 2023 Research progress in quantum key distribution *Chin. Phys. B* **32** 124207
[6] Grünenfelder F *et al* 2023 Fast single-photon detectors and real-time key distillation enable high secret-key-rate quantum key distribution systems *Nat. Photon.* **17** 422–6
[7] Giulia G *et al* 2024 Decoy-state quantum key distribution over long-distance optical fiber *Proc. SPIE* **12911** 129110D
[8] Zhu H *et al* 2024 A dynamically programmable quantum photonic microprocessor for graph computation *Laser Photon. Rev.* **18** 2300304
[9] You L 2020 Superconducting nanowire single-photon detectors for quantum information *Nanophotonics* **9** 2673–92
[10] He Y *et al* 2017 Time-bin-encoded boson sampling with a single-photon device *Phys. Rev. Lett.* **118** 190501
[11] Zhong H-S *et al* 2018 12-photon entanglement and scalable scattershot boson sampling with optimal entangled-photon pairs from parametric down-conversion *Phys. Rev. Lett.* **121** 250505
[12] Zhu D, Zhao Q-Y, Choi H, Lu T-J, Dane A E, Englund D and Berggren K K 2018 A scalable multi-photon coincidence detector based on superconducting nanowires *Nat. Nanotechnol.* **13** 596–601
[13] Reithmaier G, Kaniber M, Flassig F, Lichtmannecker S, Müller K, Andrejew A, Vučković J, Gross R and Finley J J 2015 On-chip generation, routing, and detection of resonance fluorescence *Nano Lett.* **15** 5208–13
[14] Schuck C, Pernice W H P, Ma X and Tang H X 2013 Optical time domain reflectometry with low noise waveguide-coupled superconducting nanowire single-photon detectors *Appl. Phys. Lett.* **102** 191104
[15] Zhao Q *et al* 2015 Long-haul and high-resolution optical time domain reflectometry using superconducting nanowire single-photon detectors *Sci. Rep.* **5** 10441
[16] Buschmann V *et al* 2023 Integration of a superconducting nanowire single-photon detector into a confocal microscope for time-resolved photoluminescence (TRPL)-mapping: sensitivity and time resolution *Rev. Sci. Instrum.* **94** 033703
[17] Yun M, Kai Z and Xiaolong H 2023 Superconducting nanowire single-photon detector: a rising light sensor for bio-fluorescence imaging and microscopy *Proc. SPIE* **12745** 127450Y
[18] Yamashita T, Liu D, Miki S, Yamamoto J, Haraguchi T, Kinjo M, Hiraoka Y, Wang Z and Terai H 2014 Fluorescence correlation spectroscopy with visible-wavelength superconducting nanowire single-photon detector *Opt. Express* **22** 28783–9
[19] Yu J *et al* 2020 Intravital confocal fluorescence lifetime imaging microscopy in the second near-infrared window *Opt. Lett.* **45** 3305–8
[20] Poon C-S, Rinehart B, Langri D S, Rambo T M, Miller A J, Foreman B and Sunar U 2021 Noninvasive optical monitoring of cerebral blood flow and EEG spectral responses after severe traumatic brain injury: a case report *Brain Sci.* **11** 123
[21] Piels M and Bowers J E 2023 *Photodetectors for Silicon Photonic Integrated Circuits in Photodetectors* 2nd edn, ed B Nabet (Woodhead Publishing) pp 419–36
[22] Yang W, Chen J, Zhang Y, Zhang Y, He J-H and Fang X 2019 Silicon-compatible photodetectors: trends to monolithically integrate photosensors with chip technology *Adv. Funct. Mater.* **29** 1808182
[23] Hu X, Holzwarth C W, Masciarelli D, Dauler E A and Berggren K K 2009 Efficiently coupling light to superconducting nanowire single-photon detectors *IEEE Trans. Appl. Supercond.* **19** 336–40
[24] Schuck C, Pernice W H P and Tang H X 2013 Waveguide integrated low noise NbTiN nanowire single-photon detectors with milli-Hz dark count rate *Sci. Rep.* **3** 1893
[25] Pernice W H P, Schuck C, Minaeva O, Li M, Goltsman G N, Sergienko A V and Tang H X 2012 High-speed and high-efficiency travelling wave single-photon detectors embedded in nanophotonic circuits *Nat. Commun.* **3** 1325
[26] Lomonte E, Wolff M A, Beutel F, Ferrari S, Schuck C, Pernice W H P and Lenzini F 2021 Single-photon detection and cryogenic reconfigurability in lithium niobate nanophotonic circuits *Nat. Commun.* **12** 6847
[27] Cheng R, Zhou Y, Wang S, Shen M, Taher T and Tang H X 2022 A 100-pixel photon-number-resolving detector unveiling photon statistics *Nat. Photon.* **17** 112–9
[28] PsiQuantum 2022 Silicon photonic quantum computing Towards large-scale systems Q2B SV 2022, Pete Shadbolt
[29] Alexander K, Bahgat A, Benyamini A, Black D, Bonneau D, Burgos S, Burridge B, Campbell G, Catalano G and Ceballos A 2024 A manufacturable platform for photonic quantum computing (arXiv:2404.17570)
[30] Cristiano R, Ejrnaes M, Casaburi A, Zen N and Ohkubo M 2015 Superconducting nano-strip particle detectors *Supercond. Sci. Technol.* **28** 124004
[31] Hu X, Cheng Y, Gu C, Zhu X and Liu H 2015 Superconducting nanowire single-photon detectors: recent progress *Sci. Bull.* **60** 1980
[32] Mattioli F, Zhou Z, Gaggero A, Gaudio R, Jahanmirinejad S, Sahin D, Marsili F, Leoni R and Fiore A 2015 Photon-number-resolving superconducting nanowire detectors *Supercond. Sci. Technol.* **28** 104001
[33] Miki S, Fujiwara M, Jin R-B, Yamamoto T and Sasaki M 2016 *Quantum Information Networks with Superconducting Nanowire Single-Photon Detectors Superconducting Devices in Quantum Optics* ed R H Hadfield and G Johansson (Springer) pp 107–35
[34] Najafi F, Marsili F, Verma V B, Zhao Q, Shaw M D, Berggren K K and Nam S W 2016 Superconducting nanowire architectures for single photon detection *Superconducting Devices in Quantum Optics. Superconducting Devices in Quantum Optics* ed R H Hadfield and G Johansson (Springer) pp 3–30
[35] Xiaolong H *et al* 2019 Superconducting nanowire single-photon detectors at the infrared spectrum range: detection efficiency and timing jitter *Proc. SPIE* **10917** 109171K
[36] Zhang H, Xiao L, Luo B, Guo J, Zhang L and Xie J 2020 The potential and challenges of time-resolved single-photon detection based on current-carrying superconducting nanowires *J. Phys. D: Appl. Phys.* **53** 013001
[37] Xie J and Zhang H 2024 Temporal and photon number resolution of superconducting nanowire single-photon detectors *Appl. Phys. B* **130** 113
[38] Mattioli F, Cibella S, Gaggero A, Martini F and Leoni R 2021 Waveguide-integrated niobium- nitride detectors for on-chip quantum nanophotonics *Nanotechnology* **32** 104001
[39] Pernice W H P, Schuck C and Tang H X 2016 Waveguide integrated superconducting nanowire single photon

detectors on silicon *Superconducting Devices in Quantum Optics* ed R H Hadfield and G Johansson (Springer) pp 85–105
[40] Sahin D, Gaggero A, Leoni R and Fiore A 2016 Waveguide superconducting single- and few-photon detectors on GaAs for integrated quantum photonics *Superconducting Devices in Quantum Optics* ed R H Hadfield and G Johansson (Springer) pp 61–83
[41] Ferrari S, Schuck C and Pernice W 2018 Waveguide-integrated superconducting nanowire single-photon detectors *Nanophotonics* **7** 1725
[42] Haldar S, Sehrawat A and Balasubramanian K B 2024 Modeling the effect of superconductor properties on sensitivity and responsivity of superconducting nanowire single photon detector *J. Appl. Phys.* **136** 173907
[43] Vodolazov D Y 2017 Single-photon detection by a dirty current-carrying superconducting strip based on the kinetic-equation approach *Phys. Rev. Appl.* **7** 034014
[44] Allmaras J P, Kozorezov A G, Korzh B A, Berggren K K and Shaw M D 2019 Intrinsic timing jitter and latency in superconducting nanowire single-photon detectors *Phys. Rev. Appl.* **11** 034062
[45] Semenov A D, Haas P, Günther B, Hübers H W, Il'in K and Siegel M 2008 Energy resolution of a superconducting nanowire single-photon detector *J. Low Temp. Phys.* **151** 564
[46] Semenov A D, Haas P, Hübers H-W, Ilin K, Siegel M, Kirste A and Schurig T 2008 Vortex-based single-photon response in nanostructured superconducting detectors *Physica C* **468** 627
[47] Jason P A, 2020 Modeling and development of superconducting nanowire single-photon detectors *PhD Thesis* California Institute of Technology
[48] Jahani S, Yang L-P, Buganza Tepole A, Bardin J C, Tang H X and Jacob Z 2020 Probabilistic vortex crossing criterion for superconducting nanowire single-photon detectors *J. Appl. Phys.* **127** 143101
[49] Mooij J E 1984 Two-dimensional transition in superconducting films and junction arrays *Percolation, Localization, and Superconductivity* ed A M Goldman and S A Wolf (Springer) pp 325–70
[50] Likharev K K 1979 Superconducting weak links *Rev. Mod. Phys.* **51** 101
[51] Engel A, Semenov A D, Hübers H W, Il'in K and Siegel M 2006 Fluctuation effects in superconducting nanostrips *Physica C* **444** 12
[52] Annunziata A J *et al* 2010 Reset dynamics and latching in niobium superconducting nanowire single-photon detectors *J. Appl. Phys.* **108** 084507
[53] Annunziata A J, 2010 Single-photon detection, kinetic inductance, and non-equilibrium dynamics in niobium and niobium nitride superconducting nanowires *PhD Thesis* Yale University
[54] Shainline J M, Buckley S M, Nader N, Gentry C M, Cossel K C, Cleary J W, Popović M, Newbury N R, Nam S W and Mirin R P 2017 Room-temperature-deposited dielectrics and superconductors for integrated photonics *Opt. Express* **25** 10322
[55] Clem J R and Berggren K K 2011 Geometry-dependent critical currents in superconducting nanocircuits *Phys. Rev. B* **84** 174510
[56] Henrich D, Reichensperger P, Hofherr M, Meckbach J M, Il'in K, Siegel M, Semenov A, Zotova A and Vodolazov D Y 2012 Geometry-induced reduction of the critical current in superconducting nanowires *Phys. Rev. B* **86** 144504
[57] Holzman I and Ivry Y 2019 Superconducting nanowires for single-photon detection: progress, challenges, and opportunities *Adv. Quantum Technol.* **2** 1800058
[58] Shibata H, Shimizu K, Takesue H and Tokura Y 2013 Superconducting nanowire single-photon detector with ultralow dark count rate using cold optical filters *Appl. Phys. Express* **6** 072801
[59] Lee A, Castillo A T, Whitehill C and Donaldson R 2023 Quantum bit error rate timing jitter dependency on multi-mode fibers *Opt. Express* **31** 6076
[60] *Dunbar Paul Birnie IV* 2021 Costs of detector jitter in time entanglement quantum key distribution *MSc Thesis*
[61] Xie C, Guo Y, Liao Q, Zhao W, Huang D, Zhang L and Zeng G 2018 Practical security analysis of continuous-variable quantum key distribution with jitter in clock synchronization *Phys. Lett. A* **382** 811
[62] Wu J, You L, Chen S, Li H, He Y, Lv C, Wang Z and Xie X 2017 Improving the timing jitter of a superconducting nanowire single-photon detection system *Appl. Opt.* **56** 2195
[63] Najafi F, 2015 Timing performance of superconducting nanowire single-photon detectors *PhD Thesis* Massachusetts Institute of Technology
[64] Sidorova M, Semenov A, Hübers H-W, Charaev I, Kuzmin A, Doerner S and Siegel M 2017 Physical mechanisms of timing jitter in photon detection by current-carrying superconducting nanowires *Phys. Rev. B* **96** 184504
[65] Tanner M G, Alvarez L S E, Jiang W, Warburton R J, Barber Z H and Hadfield R H 2012 Superconducting nanowire single photon detector on lithium niobate *Nanotechnology* **23** 505201
[66] Wu H, Gu C, Cheng Y and Hu X 2017 Vortex-crossing-induced timing jitter of superconducting nanowire single-photon detectors *Appl. Phys. Lett.* **111** 062603
[67] Zhao Q, Zhang L, Jia T, Kang L, Xu W, Chen J and Wu P 2011 Intrinsic timing jitter of superconducting nanowire single-photon detectors *Appl. Phys. B* **104** 673
[68] Hummel T, Widhalm A, Höpker J P, Jöns K D, Chang J, Fognini A, Steinhauer S, Zwiller V, Zrenner A and Bartley T J 2023 Nanosecond gating of superconducting nanowire single-photon detectors using cryogenic bias circuitry *Opt. Express* **31** 610
[69] Engel A and Schilling A 2013 Numerical analysis of detection-mechanism models of superconducting nanowire single-photon detector *J. Appl. Phys.* **114** 214501
[70] Engel A, Semenov A, Hübers H-W, Il'in K and Siegel M 2005 Fluctuations and dark count rates in superconducting NbN single-photon detectors *Phys. Status Solidi c* **2** 1668
[71] Semenov A, Engel A, Il'in K, Gol'tsman G, Siegel M and Hübers H W 2003 Ultimate performance of a superconducting quantum detector *Eur. Phys. J. Appl. Phys.* **21** 171
[72] Kitaygorsky J, Dorenbos S, Reiger E, Schouten R, Zwiller V and Sobolewski R 2009 HEMT-based readout technique for dark- and photon-count studies in NbN superconducting single-photon detectors *IEEE Trans. Appl. Supercond.* **19** 346
[73] Zhu D, Colangelo M, Chen C, Korzh B A, Wong F N C, Shaw M D and Berggren K K 2020 Resolving photon numbers using a superconducting nanowire with impedance-matching taper *Nano Lett.* **20** 3858
[74] Divochiy A *et al* 2008 Superconducting nanowire photon-number-resolving detector at telecommunication wavelengths *Nat. Photon.* **2** 302
[75] Jahanmirinejad S, Frucci G, Mattioli F, Sahin D, Gaggero A, Leoni R and Fiore A 2012 Photon-number resolving

detector based on a series array of superconducting nanowires *Appl. Phys. Lett.* **101** 074624
[76] Tao X *et al* 2019 A high speed and high efficiency superconducting photon number resolving detector *Supercond. Sci. Technol.* **32** 065003
[77] Natarajan C M, Zhang L, Coldenstrodt-Ronge H, Donati G, Dorenbos S N, Zwiller V, Walmsley I A and Hadfield R H 2013 Quantum detector tomography of a time-multiplexed superconducting nanowire single-photon detector at telecom wavelengths *Opt. Express* **21** 893–902
[78] Akhlaghi M K, Schelew E and Young J F 2015 Waveguide integrated superconducting single-photon detectors implemented as near-perfect absorbers of coherent radiation *Nat. Commun.* **6** 8233
[79] Vetter A *et al* 2016 Cavity-enhanced and ultrafast superconducting single-photon detectors *Nano Lett.* **16** 7085–92
[80] Münzberg J, Vetter A, Beutel F, Hartmann W, Ferrari S, Pernice W H P and Rockstuhl C 2018 Superconducting nanowire single-photon detector implemented in a 2D photonic crystal cavity *Optica* **5** 658–65
[81] Cheng R, Wang S, Zou C-L and Tang H X 2020 Design of a micrometer-long superconducting nanowire perfect absorber for efficient high-speed single-photon detection *Photon. Res.* **8** 1260–7
[82] Xiao Y, Cao X, Liu X, Jia L, Huang J, Li H, Wu A, Wang Z and You L 2023 Ultralow-filling-factor superconducting nanowire single-photon detector utilizing a 2D photonic crystal *Photon. Res.* **11** 2128–35
[83] Schwartz M, Schmidt E, Rengstl U, Hornung F, Hepp S, Portalupi S L, Ilin K, Jetter M, Siegel M and Michler P 2018 Fully on-chip single-photon Hanbury-Brown and Twiss experiment on a monolithic semiconductor–superconductor platform *Nano Lett.* **18** 6892–7
[84] Tyler N A, Barreto J, Villarreal-Garcia G E, Bonneau D, Sahin D, O'Brien J L and Thompson M G 2016 Modelling superconducting nanowire single-photon detectors in a waveguide cavity *Opt. Express* **24** 8797–807
[85] Rhazi R 2022 Development of superconducting nanowire single photon detectors integrated on silicon waveguides for quantum information *PhD Thesis.* Univ. Grenoble Alpes
[86] Sánchez-Postigo A, Graham-Scott C and Schuck C 2023 Enhancing the performance of waveguide-integrated superconducting nanowire single-photon detectors using subwavelength grating metamaterials *Proc. 23rd Int. Conf. Transparent Optical Networks (ICTON)* pp 1–4
[87] Buckley S M, Tait A N, Chiles J, McCaughan A N, Khan S, Mirin R P, Nam S W and Shainline J M 2020 Integrated-photonic characterization of single-photon detectors for use in neuromorphic synapses *Phys. Rev. Appl.* **14** 054008
[88] Sprengers J P *et al* 2011 Waveguide superconducting single-photon detectors for integrated quantum photonic circuits *Appl. Phys. Lett.* **99** 181110
[89] Sahin D *et al* 2013 Integrated autocorrelator based on superconducting nanowires *Opt. Express* **21** 11162–70
[90] Li Y *et al* 2021 Design of fabrication-tolerant and compact waveguide superconducting single-photon detector based on TM0 mode absorption *IEEE Photon. J.* **13** 1–9
[91] Xiaotian Z and Chao G, Yuhao C and Xiaolong 2015 Broadband, polarization-insensitive superconducting single-photon detectors based on waveguide-integrated ultra-narrow nanowires *Proc. Opto-Electronics and Communications Conf. (OECC)* pp 1–3
[92] Calkins B *et al* 2013 High quantum-efficiency photon-number-resolving detector for photonic on-chip information processing *Opt. Express* **21** 22657–70
[93] Kyotaro O, Tatsurou H, Tai T, Koji Y, Shinji M, Daisuke S and Hiroyuki S 2021 Si waveguide-integrated superconducting nanowire single photon detectors with arrayed waveguide grating *Proc. SPIE* **11806** 118060S
[94] Sayem A A, Cheng R, Wang S and Tang H X 2020 Lithium-niobate-on-insulator waveguide-integrated superconducting nanowire single-photon detectors *Appl. Phys. Lett.* **116** 151102
[95] Colangelo M, Desiatov B, Zhu D, Holzgrafe J, Medeiros O, Loncar M and Berggren K K 2020 Superconducting nanowire single-photon detector on thin-film lithium niobate photonic waveguide *Proc. Conf. Lasers and Electro-Optics* p SM4O.4
[96] Höpker J P *et al* 2021 Integrated superconducting nanowire single-photon detectors on titanium in-diffused lithium niobate waveguides *J. Phys.: Photon* **3** 034022
[97] Prencipe A *et al* 2023 Wavelength-sensitive superconducting single-photon detectors on thin film lithium niobate waveguides *Nano Lett.* **23** 9748–52
[98] Schuck C, Pernice W H P and Tang H X 2013 NbTiN superconducting nanowire detectors for visible and telecom wavelengths single photon counting on Si_3N_4 photonic circuits *Appl. Phys. Lett.* **102** 051101
[99] Ferrari S, Kahl O, Kovalyuk V, Goltsman G N, Korneev A and Pernice W H P 2015 Waveguide-integrated single- and multi-photon detection at telecom wavelengths using superconducting nanowires *Appl. Phys. Lett.* **106** 151101
[100] Wolff M A *et al* 2020 *Conf. Lasers Electro-Optics* p SM4O.5
[101] Korneev A, Kovalyuk V, Ferrari S, Kahl O, Pernice W, An P, Golikov A, Zubkova E and Goltsman G 2017 *Proc. 16th Int. Supercond. Electron. Conf. (ISEC)* pp 1–3
[102] Gourgues R, Zadeh I E, Elshaari A W, Bulgarini G, Los J W N, Zichi J, Dalacu D, Poole P J, Dorenbos S N and Zwiller V 2019 *Opt. Express* **27** 3710–6
[103] Kahl O, Ferrari S, Rath P, Vetter A, Nebel C and Pernice W H P 2016 *J. Lightwave Technol.* **34** 249–55
[104] Häußler M, Mikhailov M Y, Wolff M A and Schuck C 2020 *APL Photonics* **5** 076106
[105] Wolff M A, Vogel S, Splitthoff L and Schuck C 2020 *Sci. Rep.* **10** 17170
[106] Sahin D *et al* 2015 *IEEE J. Sel. Top. Quantum Electron.* **21** 1–10
[107] Gaggero A *et al* 2014 *Proc. Fotonica AEIT Italian Conference on Photonics Technologies* pp 1–4
[108] McDonald C, Moody G, Nam S W, Mirin R P, Shainline J M, McCaughan A, Buckley S and Silverman K L 2019 *Appl. Phys. Lett.* **115** 081105
[109] Patrik R, Andreas V, Vadim K, Simone F, Oliver K, Christoph N, Gregory N G, Alexander K and Wolfram H P P 2016 *Proc. SPIE* **9750** 97500T
[110] Steiner T J, Castro J E, Chang L, Dang Q, Xie W, Norman J, Bowers J E and Moody G 2021 *PRX Quantum* **2** 010337
[111] Elshaari A W, Pernice W, Srinivasan K, Benson O and Zwiller V 2020 *Nat. Photon.* **14** 285–98
[112] Bogdanov S, Shalaginov M Y, Boltasseva A and Shalaev V M 2017 *Opt. Mater. Express* **7** 111–32
[113] Shankar Kumar S and Purnima S 2018 *Emerging Waveguide Technology* ed Y Kok Yeow (IntechOpen) ch 6
[114] Giordani T, Hoch F, Carvacho G, Spagnolo N and Sciarrino F 2023 *Riv. Nuovo Cimento* **46** 71–103
[115] Luo W *et al* 2023 *Light Sci. Appl.* **12** 175
[116] Tong X C 2014 *Advanced Materials for Integrated Optical Waveguides* (Springer) pp 1–51
[117] Meng Y *et al* 2021 *Light Sci. Appl.* **10** 235
[118] Steinhauer S, Yang L, Gyger S, Lettner T, Errando-Herranz C, Jöns K D, Baghban M A, Gallo K, Zichi J and Zwiller V 2020 *Appl. Phys. Lett.* **116** 171101

[119] Banerjee A 2017 *Optimisation of Superconducting Thin Film Growth for Next Generation Superconducting Detector Applications* (University of Glasgow)

[120] Banerjee A, Heath R M, Morozov D, Hemakumara D, Nasti U, Thayne I and Hadfield R H 2018 Optical properties of refractory metal based thin films *Opt. Mater. Express* **8** 2072–88

[121] Rhazi R *et al* 2021 Improvement of critical temperature of niobium nitride deposited on 8-inch silicon wafers thanks to an AlN buffer layer *Supercond. Sci. Technol.* **34** 045002

[122] Majety S, Strohauer S, Saha P, Wietschorke F, Finley J J, Müller K and Radulaski M 2023 Triangular quantum photonic devices with integrated detectors in silicon carbide *Mater. Quantum Technol.* **3** 015004

[123] Lennon C T, Shu Y, Brennan J C, Namburi D K, Varghese V, Hemakumara D T, Longchar L A, Srinath S and Hadfield R H 2023 High-uniformity atomic layer deposition of superconducting niobium nitride thin films for quantum photonic integration *Mater. Quantum Technol.* **3** 045401

[124] Wollman E E V *et al* 2021 Recent advances in superconducting nanowire single-photon detector technology for exoplanet transit spectroscopy in the mid-infrared *J. Astron. Telesc. Instrum. Syst.* **7** 011004

[125] Hochberg Y, Charaev I, Nam S W, Verma V, Colangelo M and Berggren K K 2019 Sub-GeV dark matter with superconducting nanowires *Phys. Rev. Lett.* **123** 151802

[126] Yan X *et al* 2021 Silicon photonic quantum computing with spin qubits *APL Photonics* **6** 7

[127] Lau J A, Verma V B, Schwarzer D and Wodtke A M 2023 Superconducting single-photon detectors in the mid-infrared for physical chemistry and spectroscopy *Chem. Soc. Rev.* **52** 921–41

[128] Dello Russo S, Elefante A, Dequal D, Pallotti D K, Santamaria Amato L, Sgobba F and Siciliani de Cumis M 2022 Advances in mid-infrared single-photon detection *Photonics* **9** 47

[129] Gordon I E *et al* 2017 The HITRAN2016 molecular spectroscopic database *J. Quant. Spectrosc. Radiat. Transfer* **203** 3–69

[130] Goltsman Y K, Il'in F A and Semenov A K 2010 New generation of nanowire NbN superconducting single-photon detector for mid-infrared *IEEE Trans. Appl. Supercond.* **21** 323–6

[131] Marsili F, Najafi F, Dauler E, Bellei F, Hu X, Csete M, Molnar R J and Berggren K K 2011 Single-photon detectors based on ultranarrow superconducting nanowires *Nano Lett.* **11** 2048–53

[132] Korneev A, Korneeva Y, Florya I, Voronov B and Goltsman G 2012 NbN nanowire superconducting single-photon detector for mid-infrared *Phys. Proc.* **36** 72–76

[133] Marsili F, Bellei F, Najafi F, Dane A E, Dauler E A, Molnar R J and Berggren K K 2012 Efficient single photon detection from 500 nm to 5 μm wavelength *Nano Lett.* **12** 4799–804

[134] Chang J, Los J W N, Gourgues R, Steinhauer S, Dorenbos S N, Pereira S F, Urbach H P, Zwiller V and Esmaeil Zadeh I 2022 Efficient single photon detection from 500 nm to 5 mum wavelength *Photon. Res.* **10** 4

[135] Taylor G G, MacKenzie E N, Korzh B, Morozov D V, Bumble B, Beyer A D, Allmaras J P, Shaw M D and Hadfield R H 2022 Mid-infrared timing jitter of superconducting nanowire single-photon detectors *Appl. Phys. Lett.* **121** 21

[136] Dorenbos S N, Forn-Díaz P, Fuse T, Verbruggen A H, Zijlstra T, Klapwijk T M and Zwiller V 2011 Low gap superconducting single photon detectors for infrared sensitivity *Appl. Phys. Lett.* **98** 25

[137] Baek B, Lita A E, Verma V and Nam S W 2011 Superconducting a-W_xSi_{1-x} nanowire single-photon detector with saturated internal quantum efficiency from visible to 1850 nm *Appl. Phys. Lett.* **98** 25

[138] Engel A, Aeschbacher A, Inderbitzin K, Schilling A, Il'in K, Hofherr M, Siegel M, Semenov A and Hübers H W 2012 Tantalum nitride superconducting single-photon detectors with low cut-off energy *Appl. Phys. Lett.* **100** 6

[139] Chen Q *et al* 2021 Mid-infrared single photon detector with superconductor $Mo_{0.8}Si_{0.2}$ nanowire *Sci. Bull.* **66** 965–8

[140] Wolf S and Lowrey W H 1977 Zero dimensionality and Josephson coupling in granular niobium nitride *Phys. Rev. Lett.* **39** 1038–41

[141] Kang J, Yang X, Hu Q, Cai Z, Liu L-M and Guo L 2023 Recent progress of amorphous nanomaterials *Chem. Rev.* **123** 8859–941

[142] Banerjee A, Baker L J, Doye A, Nord M, Heath R M, Erotokritou K, Bosworth D, Barber Z H, MacLaren I and Hadfield R H 2017 Characterisation of amorphous molybdenum silicide (MoSi) superconducting thin films and nanowires *Supercond. Sci. Technol.* **30** 084010

[143] Verma V B, Marsili F, Harrington S, Lita A E, Mirin R P and Nam S W 2012 A three-dimensional, polarization-insensitive superconducting nanowire avalanche photodetector *Appl. Phys. Lett.* **101** 251114

[144] Bosworth D, Sahonta S L, Hadfield R H and Barber Z H 2015 Amorphous molybdenum silicon superconducting thin films *AIP Adv.* **5** 087106

[145] Shibata H 2021 Review of superconducting nanostrip photon detectors using various superconductors *IEICE Trans. Electron.* **E104.C** 429–34

[146] Korzh B *et al* 2018 WSi superconducting nanowire single-photon detector with a temporal resolution below 5 ps *Conf. Lasers Electro-Optics* (*San Jose*)

[147] Verma V B, Lita A E, Vissers M R, Marsili F, Pappas D P, Mirin R P and Nam S W 2014 Superconducting nanowire single photon detectors fabricated from an amorphous $Mo_{0.75}Ge_{0.25}$ thin film *Appl. Phys. Lett.* **105** 022602

[148] Reddy D V, Nerem R R, Nam S W, Mirin R P and Verma V B 2020 Superconducting nanowire single-photon detectors with 98% system detection efficiency at 1550 nm *Optica* **7** 1649

[149] Pan Y, Zhou H, Zhang X, Yu H, Zhang L, Si M, Li H, You L and Wang Z 2022 Mid-infrared Nb4_44 N3_33-based superconducting nanowire single photon detectors for wavelengths up to 10 μm *Opt Express* **30** 40044–52

[150] Pan Y, Zhou H, Zhang L, Li H, Tang Y, Yu H, Si M, You L and Wang Z 2021 Superconducting nanowire single-photon detector made of ultrathin γ-Nb4_44 N3_33 film for mid-infrared wavelengths *Supercond. Sci. Technol.* **34** 075010

[151] Verma V B *et al* 2021 Single-photon detection in the mid-infrared up to 10 μm wavelength using tungsten silicide superconducting nanowire detectors *APL Photonics* **6** 056114

[152] Colangelo M *et al* 2022 Large-area superconducting nanowire single-photon detectors for operation at wavelengths up to 7.4 μm *Nano Lett.* **22** 5667–73

[153] Taylor G G, Walter A B, Korzh B, Bumble B, Patel S R, Allmaras J P, Beyer A D, O'Brient R, Shaw M D and Wollman E E 2023 Low-noise single-photon counting superconducting nanowire detectors at infrared wavelengths up to 29 μm *Optica* **10** 1409–15

[154] Ivry Y, Surick J J, Barzilay M, Kim C-S, Najafi F, Kalfon-Cohen E, Dane A D and Berggren K K 2017 Superconductor-superconductor bilayers for enhancing single-photon detection *Nanotechnology* **28** 435205

[155] Charaev I *et al* 2022 Single-photon detection using high-temperature superconductors *Nat. Nanotechnol.* **18** 343–9
[156] Velasco A E *et al* 2017, High-operating-temperature superconducting nanowire single photon detectors based on magnesium diboride *Conf. Lasers Electro-Optics* (*San Jose*)
[157] Arpaia R, Ejrnaes M, Parlato L, Cristiano R, Arzeo M, Bauch T, Nawaz S, Tafuri F, Pepe G P and Lombardi F 2014 Highly homogeneous YBCO/LSMO nanowires for photoresponse experiments *Supercond. Sci. Technol.* **27** 044027
[158] Hunsperger R G and Lee A 1976 Parallel end-butt coupling of a GaAs laser diode and a thin film waveguide *Integrated Optics* (*Optica Publishing Group*) p WD4
[159] Parmar V, Bhatnagar R and Kapur P 2013 Optimized butt coupling between single-mode fiber and hollow-core photonic crystal fiber *Opt. Fiber Technol.* **19** 490–4
[160] Son G, Han S, Park J, Kwon K and Yu K 2018 High-efficiency broadband light coupling between optical fibers and photonic integrated circuits *Nanophotonics* **7** 1845–64
[161] Wolff M A, Beutel F, Schütte J, Gehring H, Häußler M, Pernice W and Schuck C 2021 Broadband waveguide-integrated superconducting single-photon detectors with high system detection efficiency *Appl. Phys. Lett.* **118** 154004
[162] Häußler M *et al* 2023 Scaling waveguide-integrated superconducting nanowire single-photon detector solutions to large numbers of independent optical channels *Rev. Sci. Instrum.* **94** 013103
[163] Billah M *et al* 2018 Hybrid integration of silicon photonics circuits and InP lasers by photonic wire bonding *Optica* **5** 876–83
[164] Lin B, Witt D, Young J F and Chrostowski L 2023 Cryogenic optical packaging using photonic wire bonds *APL Photonics* **8** 126109
[165] Gehring H, Eich A, Schuck C and Pernice W H P 2019 Broadband out-of-plane coupling at visible wavelengths *Opt. Lett.* **44** 5089–92
[166] Rosfjord K M, Yang J K W, Dauler E A, Kerman A J, Anant V, Voronov B M, Gol'tsman G N and Berggren K K 2006 Nanowire single-photon detector with an integrated optical cavity and anti-reflection coating *Opt. Express* **14** 527–34
[167] Eftekharian A 2014 Plasmonic superconducting single photon detector *PhD Thesis* University of Waterloo
[168] Matteo C *et al* 2023 Supporting quantum technologies with an ultralow-loss silicon photonics platform *Proc. SPIE* **2** 024002
[169] Dai Y *et al* 2023 All-fiber device for single-photon detection *PhotoniX* **4** 7
[170] Najafi F *et al* 2015 On-chip detection of non-classical light by scalable integration of single-photon detectors *Nat. Commun.* **6** 5873
[171] Errando-Herranz C *et al* 2023 Transfer-printed single-photon detectors on arbitrary photonic substrates *Conf. Lasers Electro-Optics* **2023** 1–2
[172] Chen S *et al* 2022 Stacking two superconducting nanowire single-photon detectors via membrane microchip transfer *Appl. Phys. Lett.* **121** 112601
[173] McPhillimy J, Jevtics D, Guilhabert B J E, Klitis C, Hurtado A, Sorel M, Dawson M D and Strain M J 2020 Automated nanoscale absolute accuracy alignment system for transfer printing *ACS Appl. Nano Mater.* **3** 10326–32
[174] Meitl M A, Zhu Z-T, Kumar V, Lee K J, Feng X, Huang Y Y, Adesida I, Nuzzo R G and Rogers J A 2006 Transfer printing by kinetic control of adhesion to an elastomeric stamp *Nat. Mater.* **5** 33–38
[175] Sahin D *et al* 2013 Waveguide-integrated single- and multi-photon detection at telecom wavelengths using superconducting nanowires *Appl. Phys. Lett.* **103** 111116
[176] Gaggero A, Martini F, Mattioli F, Chiarello F, Cernansky R, Politi A and Leoni R 2019 Amplitude-multiplexed readout of single photon detectors based on superconducting nanowires *Optica* **6** 823–8
[177] Sahin D *et al* 2013 Waveguide photon-number-resolving detectors for quantum photonic integrated circuits *Appl. Phys. Lett.* **103** 111116
[178] PsiQuantum 2022 Photon number resolving superconducting detector *US Patent*
[179] Knill E, Laflamme R and Milburn G J 2001 A scheme for efficient quantum computation with linear optics *Nature* **409** 46–52
[180] Gottesman D, Kitaev A and Preskill J 2001 Encoding a qubit in an oscillator *Phys. Rev. A* **64** 012310
[181] Bourassa J E *et al* 2021 Blueprint for a scalable photonic fault-tolerant quantum computer *Quantum* **5** 392
[182] Hampel B, Slichter D H, Leibfried D, Mirin R P, Nam S W and Verma V B 2023 Trap-integrated superconducting nanowire single-photon detectors with improved RF tolerance for trapped-ion qubit state readout *Appl. Phys. Lett.* **122** 172601
[183] Todaro S L, Verma V B, McCormick K C, Allcock D T C, Mirin R P, Wineland D J, Nam S W, Wilson A C, Leibfried D and Slichter D H 2021 State readout of a trapped ion qubit using a trap-integrated superconducting photon detector *Phys. Rev. Lett.* **126** 010501
[184] Simmons S 2024 Scalable fault-tolerant quantum technologies with silicon color centers *PRX Quantum* **5** 010102
[185] Pirandola S *et al* 2020 Advances in quantum cryptography *Adv. Opt. Photon.* **12** 1012–236
[186] Shen X, Xu B and Wu W 2019 The review of the commercial quantum key distribution system *Proc. 2019 IEEE 4th Int. Conf. Comput. Commun. Syst. (ICCCS)* (*Singapore*, *23–25 February 2019*) pp 700–4
[187] Oesterling L, Hayford D and Friend G, 2012 *Proc. 2012 IEEE Conf. Technol. Homeland Secur* **2012** pp 6459842
[188] Xu F, Ma X, Zhang Q, Lo H-K and Pan J-W 2020 Secure quantum key distribution with realistic devices *Rev. Mod. Phys.* **92** 025002
[189] Mehic M *et al* 2020 Quantum key distribution *ACM Comput. Surv.* **53** 1–41
[190] Liu Q, Huang Y, Du Y, Zhao Z, Geng M, Zhang Z and Wei K 2022 Advances in chip-based quantum key distribution *Entropy* **24** 1334
[191] Koziy A A, Losev A V, Zavodilenko V V, Kurochkin Y V and Gorbatsevich A A 2021 Modern methods of detecting single photons and their application in quantum communications *Quantum Electron.* **51** 655
[192] Beutel F, Gehring H, Wolff M A, Schuck C and Pernice W 2021 Detector-integrated on-chip QKD receiver for GHz clock rates *npj Quantum Inf.* **7** 40
[193] Zheng X *et al* 2021 Heterogeneously integrated, superconducting silicon-photonic platform for measurement-device-independent quantum key distribution *Adv. Photon.* **3** 055002
[194] Beutel F, Brückerhoff-Plückelmann F, Gehring H, Kovalyuk V, Zolotov P, Goltsman G and Pernice W H P 2022 Fully integrated four-channel wavelength-division multiplexed QKD receiver *Optica* **9** 1121
[195] Terhaar R *et al* 2023 Ultrafast quantum key distribution using fully parallelized quantum channels *Opt Express* **31** 2675–88
[196] Villegas-Aguilar L *et al* 2024 Nonlocality activation in a photonic quantum network *Nat. Commun.* **15** 3112

[197] Couteau C, Barz S, Durt T, Gerrits T, Huwer J, Prevedel R, Rarity J, Shields A and Weihs G 2023 Applications of single photons in quantum metrology, biology and the foundations of quantum physics *Nat. Rev. Phys.* **5** 354–63
[198] Manning A G, Khakimov R I, Dall R G and Truscott A G 2015 Wheeler's delayed-choice gedanken experiment with a single atom *Nat. Phys.* **11** 539–42
[199] Bracken C P and McAleer C 2022 A delayed-choice quantum eraser with photon-counting MKIDs (experimental design) *J. Low Temp. Phys.* **209** 899–911
[200] Zivari A, Fiaschi N, Burgwal R, Verhagen E, Stockill R and Gröblacher S 2022 On-chip distribution of quantum information using traveling phonons *Sci. Adv.* **8** eadd2811
[201] Zivari A, Stockill R, Fiaschi N and Gröblacher S 2022 Non-classical mechanical states guided in a phononic waveguide *Nat. Phys.* **18** 789–93
[202] Yu Y *et al* 2020 Entanglement of two quantum memories via fibres over dozens of kilometres *Nature* **578** 240–5
[203] Yuan Z-S, Chen Y-A, Zhao B, Chen S, Schmiedmayer J and Pan J-W 2008 Experimental demonstration of a BDCZ quantum repeater node *Nature* **454** 1098–101
[204] Azuma K, Economou S E, Elkouss D, Hilaire P, Jiang L, Lo H-K and Tzitrin I 2023 Quantum repeaters: from quantum networks to the quantum internet *Rev. Mod. Phys.* **95** 045006
[205] Bhaskar M K *et al* 2020 Experimental demonstration of memory-enhanced quantum communication *Nature* **580** 60–64
[206] Wallucks A, Marinković I, Hensen B, Stockill R and Gröblacher S 2020 A quantum memory at telecom wavelengths *Nat. Phys.* **16** 772–7
[207] Cheng R, Zou C-L, Guo X, Wang S, Han X and Tang H X 2019 Broadband on-chip single-photon spectrometer *Nat. Commun.* **10** 4104
[208] le Coarer E, Blaize S, Benech P, Stefanon I, Morand A, Lérondel G, Leblond G, Kern P, Fedeli J M and Royer P 2007 Wavelength-scale stationary-wave integrated Fourier-transform spectrometry *Nat. Photon.* **1** 473–8
[209] Cavalier P, Constancias C, Feautrier P, Maingault L, Morand A and Villegier J C 2011 SWIFTS waveguide micro-spectrometer integrated on top of a 1D-NbN SNSPD array *IEEE Trans. Appl. Supercond.* **21** 327–31
[210] Cavalier P, Villégier J-C, Feautrier P, Constancias C and Morand A 2011 Light interference detection on-chip by integrated SNSPD counters *AIP Adv.* **1** 042120
[211] Elshaari A W, Iovan A, Gyger S, Zadeh I E, Zichi J, Yang L, Steinhauer S and Zwiller V 2020 Dispersion engineering of superconducting waveguides for multi-pixel integration of single-photon detectors *APL Photonics* **5** 111301
[212] Rank E A *et al* 2021 Toward optical coherence tomography on a chip: *in vivo* three-dimensional human retinal imaging using photonic integrated circuit-based arrayed waveguide gratings *Light Sci. Appl.* **10** 6
[213] Bingham R G 1979 Grating spectrometers and spectrographs re-examined *Q J. R. Astron. Soc.* **20** 395–421
[214] Zheng J, Xiao Y, Hu M, Li H, You L, Feng X, Liu F, Cui K, Huang Y and Zhang W 2023 An on-chip photon-counting reconstructive spectrometer with tailored cascaded detector array *Adv. Dev. Instrum.* **4** 0021
[215] Cao H and Eliezer Y 2022 Harnessing disorder for photonic device applications *Appl. Phys. Rev.* **9** 011309
[216] Rothammer M, Zollfrank C, Busch K and von Freymann G 2021 Tailored disorder in photonics: learning from nature *Adv. Opt. Mater.* **9** 2100787
[217] Gupta R K, Bruce G D, Powis S J and Dholakia K 2020 Deep learning enabled laser speckle wavemeter with a high dynamic range *Laser Photon. Rev.* **14** 2000120
[218] Israelsen N M, Petersen C R, Barh A, Jain D, Jensen M, Hannesschläger G, Tidemand-Lichtenberg P, Pedersen C, Podoleanu A and Bang O 2019 Real-time high-resolution mid-infrared optical coherence tomography *Light Sci. Appl.* **8** 11
[219] Colley C S, Hebden J C, Delpy D T, Cambrey A D, Brown R A, Zibik E A, Ng W H, Wilson L R and Cockburn J W 2007 Mid-infrared optical coherence tomography *Rev. Sci. Instrum.* **78** 123108
[220] Banu K S, Lerma M, Ahmed S U and Gardea-Torresdey J L 2024 Hyperspectral microscopy—applications of hyperspectral imaging techniques in different fields of science: a review of recent advances *Appl. Spectrosc. Rev.* **59** 935–58
[221] Hermes M *et al* 2018 Mid-IR hyperspectral imaging for label-free histopathology and cytology *J. Opt.* **20** 023002
[222] Wang F *et al* 2022 *In vivo* non-invasive confocal fluorescence imaging beyond 1,700 nm using superconducting nanowire single-photon detectors *Nat. Nanotechnol.* **17** 653–60
[223] Gemmell N R, McCarthy A, Liu B, Tanner M G, Dorenbos S D, Zwiller V, Patterson M S, Buller G S, Wilson B C and Hadfield R H 2013 Singlet oxygen luminescence detection with a fiber-coupled superconducting nanowire single-photon detector *Opt. Express* **21** 5005–13
[224] Tsimvrakidis K, Gemmell N R, Erotokritou K, Miki S, Yabuno M, Yamashita T, Terai H and Hadfield R H 2019 Enhanced optics for time-resolved singlet oxygen luminescence detection *IEEE J. Sel. Top. Quantum Electron.* **25** 1–7
[225] Selvaraj R, Vasa N J, Nagendra S M S and Mizaikoff B 2020 Advances in mid-infrared spectroscopy-based sensing techniques for exhaled breath diagnostics *Molecules* **25** 2227
[226] Biamonte J, Wittek P, Pancotti N, Rebentrost P, Wiebe N and Lloyd S 2017 Quantum machine learning *Nature* **549** 195–202
[227] Ciliberto C, Herbster M, Ialongo A D, Pontil M, Rocchetto A, Severini S and Wossnig L 2018 Quantum machine learning: a classical perspective *Proc. R. Soc. A* **474** 20170551
[228] Ren M, Gu X, Liang Y, Kong W, Wu E, Wu G and Zeng H 2011 Laser ranging at 1550 nm with 1-GHz sine-wave gated InGaAs/InP APD single-photon detector *Opt Express* **19** 13497–502
[229] Xia H *et al* 2015 Long-range micro-pulse aerosol lidar at 1.5 μm with an upconversion single-photon detector *Opt. Lett.* **40** 1579–82
[230] Zhu J *et al* 2017 Demonstration of measuring sea fog with an SNSPD-based Lidar system *Sci. Rep.* **7** 15113
[231] Zhang J, Sua Y M, Chen J-Y, Ramanathan J, Tang C, Li Z, Hu Y and Huang Y-P 2021 Carbon-dioxide absorption spectroscopy with solar photon counting and integrated lithium niobate micro-ring resonator *Appl. Phys. Lett.* **118** 177
[232] Luo W, Wu C, Du Y, Zhao C, Yu M, Zhu P, Zhang K and Xu P 2024 On-chip quantum NOON state sensing for temperature and humidity *Chin. Phys. B* **33** 100305
[233] Taylor G G, Morozov D V, Lennon C T, Barry P S, Sheagren C and Hadfield R H 2021 Infrared single-photon sensitivity in atomic layer deposited superconducting nanowires *Appl. Phys. Lett.* **118** 192601
[234] Cheng R, Wright J, Xing H G, Jena D and Tang H X 2020 Epitaxial niobium nitride superconducting nanowire single-photon detectors *Appl. Phys. Lett.* **117** 132602
[235] Zhang W, Jia Q, You L, Ou X, Huang H, Zhang L, Li H, Wang Z and Xie X 2019 Saturating intrinsic detection

efficiency of superconducting nanowire single-photon detectors via defect engineering *Phys. Rev. Appl.* **12** 044040
[236] Strohauer S *et al* 2024 Site-selective enhancement of superconducting nanowire single-photon detectors via local helium ion irradiation *Adv. Quantum Technol.* **6** 2200139
[237] Azem A, Morozov D V, Kuznesof D, Bruscino C, Hadfield R H, Chrostowski L and Young J F 2024 Mid-infrared characterization of NbTiN superconducting nanowire single-photon detectors on silicon-on-insulator *Appl. Phys. Lett.* **125** 212602
[238] Castellani M, Medeiros O, Foster R A, Buzzi A, Colangelo M, Bienfang J C, Restelli A and Berggren K K 2024 Nanocryotron ripple counter integrated with a superconducting nanowire single-photon detector for megapixel arrays *Phys. Rev. Appl.* **22** 024020
[239] Steinhauer S, Gyger S and Zwiller V 2021 Progress on large-scale superconducting nanowire single-photon detectors *Appl. Phys. Lett.* **118** 100501
[240] Thiele F, Lamberty N, Hummel T and Bartley T 2024 Optical bias and cryogenic laser readout of a multipixel superconducting nanowire single-photon detector *APL Photonics* **9** 076118
[241] Tiedau J, Schapeler T, Anant V, Fedder H, Silberhorn C and Bartley T J 2020 Single-channel electronic readout of a multipixel superconducting nanowire single photon detector *Opt Express* **28** 5528–37
[242] Wollman E E, Allmaras J P, Verma V B, de Cea M, Korzh B, Atabaki A H, Ram R J, Nam S W and Shaw M D 2020 Advances in readout techniques for arrays of superconducting nanowire single-photon detectors *Conf. Lasers Electro-Opt* vol 2020 p FF3D.1
[243] Oripov B G, Rampini D S, Allmaras J, Shaw M D, Nam S W, Korzh B and McCaughan A N 2023 A superconducting nanowire single-photon camera with 400,000 pixels *Nature* **622** 730–4
[244] Doylend J K and Gupta S 2020 An overview of silicon photonics for LIDAR *Proc. SPIE* **11285** 112850J
[245] Ahmadi S, Saglamyurek E, Barzanjeh S and Salari V 2023 High-contrast interaction-free quantum imaging method *Phys. Rev. A* **107** 032611
[246] Yang Y, Liang H, Xu X, Zhang L, Zhu S and Ma X-S 2023 Interaction-free, single-pixel quantum imaging with undetected photons *npj Quantum Inf.* **9** 2